



TAMPEREEN TEKNILLINEN YLIOPISTO  
TAMPERE UNIVERSITY OF TECHNOLOGY

Karoliina Koski

**Characterization and Design Methodologies for Wearable  
Passive UHF RFID Tag Antennas for Wireless Body-  
Centric Systems**



Julkaisu 1274 • Publication 1274

Tampereen teknillinen yliopisto. Julkaisu 1274  
Tampere University of Technology. Publication 1274

Karoliina Koski

## **Characterization and Design Methodologies for Wearable Passive UHF RFID Tag Antennas for Wireless Body- Centric Systems**

Thesis for the degree of Doctor of Science in Technology to be presented with due permission for public examination and criticism in Sähköotalo Building, Auditorium SM221, at Tampere University of Technology, on the 23<sup>rd</sup> of January 2015, at 12 noon.

Tampereen teknillinen yliopisto - Tampere University of Technology  
Tampere 2015

ISBN 978-952-15-3434-8 (printed)  
ISBN 978-952-15-3441-6 (PDF)  
ISSN 1459-2045

## ABSTRACT

Radio Frequency Identification (RFID) is a wireless automatic identification technology that utilizes electrically active tags – low-cost and low-power wireless communication devices that let themselves transparently and unobstructively be embedded into everyday objects to remotely track information of the object’s physical location, origin, and ownership. At ultra-high frequencies (UHF), this technology uses propagating electromagnetic waves for communication, which enables the fast identification of tags at large distances. A passive RFID tag includes two main components; a tag antenna and an RFID integrate circuit (tag IC). A passive tag relies solely on the external power harvested from an incident electromagnetic wave to run its circuitry and for data transmission. The passiveness makes the tag maintenance-free, simple, and low-cost, allowing large-scale commercial applications in the supply chain, ticketing, and asset tracking. The future of RFID, however, lies in the transition from traditional embedded applications to wearable intelligent systems, in which the tags are seamlessly integrated with everyday clothing. Augmented with various ambient and biochemical sensors, the tag is capable of detecting physical parameters of its environment and providing continuous monitoring of human vital signs. Tremendous amount of tagged entities establish an intelligent infrastructure that is personalized and tailored to the needs of each individual and ultimately, it recedes into the background of our daily life.

Although wearable tags in intelligent systems have the enormous potential to revolutionize the quality of human life, the emerging wearable RFID applications introduce new challenges for designers developing efficient and sophisticated RFID systems. Traditional tag design parameters and solutions will no longer respond to the new requirements. Instead, the whole RF community must adopt new methods and unconventional approaches to achieve advanced wearable tags that are highly transparently integrated into our daily life.

In this research work, an empirical as well as a theoretical approach is taken to address the above-mentioned wearable RFID tag challenges. Exploiting new analysis tools in combination with computational electromagnetics, a novel technique to model the human body in UHF applications for initiating the design of optimized wearable tags is developed. Further, fundamental unprecedented UHF characteristics of advanced wearable electronics materials – electro-textiles, are established. As an extremely important outcome of this research work, innovative optimization methodologies for the promotion of novel and advanced wearable UHF antennas are proposed. Particularly, it is evidenced that proper embroidery fabrication techniques have the great potential to realize wearable tag antennas exhibiting excellent RF performance and structural properties for the seamless integration with clothing. The kernel of this research work is the realization of a flexible and fully embroidered passive UHF RFID patch tag prototype achieving optimized performance in close vicinity of the high-permittivity and dissipative human body. Its performance may be considered as a benchmark for future wearable antenna designs. This shows that this research work outcome forms an important contribution to the state of the art and a milestone in the development towards wearable intelligence.



## PREFACE

This research work was carried out at the Department of Electronics and Communications Engineering, Tampere University of Technology, Wireless Identification and Sensing Systems (WISE) Research Group during the years 2012–2014. The research was funded by the Finnish Funding Agency for Technology and Innovation (TEKES), the Academy of Finland, the Centennial Foundation of Finnish Technology Industries, KAUTE foundation, Nokia Foundation, Emil Aaltosen Foundation, Tekniikan Edistämissäätiö Foundation, and Ulla Tuomisen Foundation. The financial support is gratefully acknowledged.

I would like to thank my supervisor Prof. Leena Ukkonen and my advisor the Head of the Department of Electronics and Communications Engineering Lauri Sydänheimo at Tampere University of Technology for granting me the opportunity to complete my doctoral studies in their research group. I greatly appreciate their encouragement, guidance, and belief in me during my doctoral studies. I am also sincerely grateful to Prof. Yahya Rahmat-Samii from the University of California, Los Angeles, for his outstanding and constructive feedback and critics. I wish to express my gratitude to Academy Research Fellow, Associate Prof. Elena-Simona Lohan for all her support and excellent co-operation. I want to thank my opponent Prof. Anja Skrivervik and my pre-examiners Associate Prof. Jorge Costa and Prof. Hendrik Rogier for criticizing and examining my thesis.

My sincerest appreciation goes to my colleagues in WISE Research Group. I especially want to thank Dr. Toni Björninen and Elham Moradi for the valuable discussions and their significant input to my research work. A special thanks goes to Associate Prof. Arnaud Vena for being a professional and dedicated researcher and a great source of inspiration. I wish him great success in his future endeavors. I also wish all the best to my new and old colleagues in WISE Research Group. Thanks to Dr. Abdul Ali Babar for all his support and for the laughs we had during my doctoral studies.

I would like to express my deepest gratitude to my father and mother for their endless patience, understanding, and love. Still, above all, I want to thank my loving fiancé Tuomas Messo for standing by me and believing in me. Finally, I am grateful to my sister Eveliina Koski for being the biggest support in my life, an honest person that pushes me beyond my own limits, and giving me the confidence to reach my goals.

Tampere, December 2014

Karoliina Koski

## LIST OF PUBLICATIONS

- [I] E. Moradi, K. Koski, T. Björninen, L. Sydänheimo, J. M. Rabaey, J. M. Carmena, Y. Rahmat-Samii, L. Ukkonen, “Miniature implantable and wearable on-body antennas: towards the new era of wireless body-centric systems,” *Invited paper in IEEE Antennas and Propagation Magazine, Antenna Applications Corner*, vol. 56, no. 1, pp. 271–291, February 2014.
- [II] K. Koski, T. Björninen, L. Sydänheimo, L. Ukkonen, Y. Rahmat-Samii, “A new approach and analysis of modeling the human body in RFID-enabled body-centric wireless systems,” *International Journal of Antennas and Propagation*, vol. 2014, Article ID 368090, 12 p., April 2014.
- [III] K. Koski, A. Vena, L. Sydänheimo, L. Ukkonen, Y. Rahmat-Samii, “Design and implementation of electro-textile ground planes for wearable UHF RFID patch tag antennas,” *IEEE Antennas and Wireless Propagation Letters*, vol. 12, no. 1, pp. 964–967, December 2013.
- [IV] K. Koski, L. Sydänheimo, Y. Rahmat-Samii, L. Ukkonen, “Fundamental characteristics of electro-textiles in wearable UHF RFID patch antennas for body-centric sensing systems,” *IEEE Transaction on Antennas and Propagation*, vol. 62, no. 12, 9 p., December 2014.
- [V] K. Koski, E. S. Lohan, L. Sydänheimo, L. Ukkonen, Y. Rahmat-Samii, “Electro-textile UHF RFID patch antennas for positioning and localization applications,” *IEEE International Conference on RFID Technology and Applications*, pp. 246–250, Tampere, Finland, 8–9 September, 2014.

## **AUTHOR'S CONTRIBUTION**

- [I] The author and co-author Elham Moradi are the main contributors of the work. The author has contributed the publication section 3 and is the main contributor of the section 3 publication text. Elham Moradi has contributed the publication section 2 and is the main contributor of the section 2 publication text. This publication presents all antenna aspects required in novel body-centric communication systems. The author has concentrated on electro-textile on-body antennas, whereas co-author Elham Moradi has concentrated on extremely small implant antennas and wireless link optimization through tissue. Therefore, contribution of both of the main authors has been equally wide and in-depth. Role of all the other authors (T. Björninen, L. Sydänheimo, J. M. Rabaey, J. M. Carmena, Y. Rahmat-Samii, L. Ukkonen) has been advisory.
- [II] The modeling technique was developed by the author. The author designed and fabricated the prototype tags, conducted all simulations, and is the main contributor of the publication text. The on-body measurements were conducted in co-operation with Mikko Toivonen. The post-processing of the measurement results were performed in co-operation with Dr. Toni Björninen.
- [III] The author designed and fabricated the reference patch tag. The presented tag antenna electro-textile ground plane prototypes were designed, fabricated, and measured by the author. The wireless reflectometry measurements were conducted and the measurement data was post-processed in co-operation with Associate Prof. Arnaud Vena. The author fabricated and simulated the reference patch tag with electro-textile ground plane and is the main contributor of the publication text.
- [IV] The author has contributed the publication contents and is the main contributor of the publication text.
- [V] The author designed and fabricated the prototype tags. The author prepared the measurement set-up and conducted all the measurements. The signal processing was performed in co-operation with Academy Research Fellow, Associate Prof. Elena-Simona Lohan. The author is the main contributor of the publication text.



## CONTENTS

ABSTRACT.....	i
PREFACE.....	iii
LIST OF PUBLICATIONS.....	iv
AUTHOR'S CONTRIBUTION.....	v
CONTENTS.....	vi
1 Introduction.....	1
1.1 Wearable intelligence – The new era of wireless body-centric systems.....	1
1.2 The passive UHF RFID system.....	2
1.3 Scope and objectives of the thesis.....	5
1.4 Structure of the thesis.....	5
2 Passive UHF RFID Tag Design Parameters and Performance Metrics.....	7
2.1 Antenna radiation characteristics.....	8
2.2 Tag antenna impedance matching and antenna scattering.....	10
2.3 Performance indicators.....	13
2.4 Microstrip patch antenna.....	15
2.5 Modeling methodology for the human body in UHF body-centric systems.....	18
3 Wearable Antennas in Wireless Body-Centric Systems.....	25
3.1 Wearable antenna design challenges.....	26
3.2 Electro-textiles for seamless and robust integration with clothing.....	26
3.3 Embroidered antenna durability.....	28
4 Fundamental Characteristics of Electro-Textiles for Wearable UHF Antennas.....	30
4.1 Case study 1: Electro-textiles for which $Z_S$ is real.....	33
4.2 Case study 2: Electro-textiles for which $Z_S$ is complex.....	34
4.3 Case study 3: Electro-textile UHF RFID patch tags for wearable applications.....	39
5 Conclusions.....	47
REFERENCES.....	49

## 1 INTRODUCTION

With the vision of a global infrastructure of networked intelligent physical objects, various concepts that interconnect the physical world with the virtual one have emerged [1][2][3][4][5]. Internet of Things (IoT) is currently the most recognized paradigm, a futuristic vision in which the Internet embeds itself into everyday objects in a transparent and an unobtrusive manner [2]. The intelligence is brought to the smart objects by augmenting them with sensing and computing capabilities, allowing them to sense, interpret, and act on their environment, intercommunicate and change information with each other and with people. This way, the human become part of the feedback loop of a computational entity in which the computer and human are inextricably intertwined [1][4]. Such envisaged pervasive computing is personalized and tailored to the needs of each individual and ultimately, it recedes into the background of our daily life. This *disappearance* of the technology was already predicted in 1991 by Mark Weiser as a fundamental consequence of the seamless integration of computational intelligence into the world [6].

### 1.1 Wearable intelligence – The new era of wireless body-centric systems

The vision of an ubiquitous intelligent environment is greatly inspired by the success of wireless body-centric systems [4][7][8]. They are considered as an important part of the fourth generation mobile communication systems and are expected to be part of the future convergence and personalization of the personal area networks (PANs) and body area networks (BANs) [4][7]. The scaling of CMOS device technology has made it possible to integrate computing features in a tremendous amount of devices. Today, we are surrounded by various computing devices such as personal computers, smart phones, Global Positioning Systems (GPS), tablets, and numerous sensor devices used for example in remotely controlled home applications. The new trend, however, is the transition from traditional embedded applications to wearable applications, in which sensing and computing devices are seamlessly integrated with everyday clothing. This new technology is expected to offer unique applications for consumer electronics, military industries, human localization services, and personal healthcare and wellbeing services [8][9][10]. When biomedical sensor devices become wirelessly wearable, continuous monitoring of human vital signs will revolutionize the quality of human life. Most diseases can be prevented if they are detected in their early stages. Proactive healthcare management through wearable monitoring systems holds an enormous potential to help people suffering from abnormal conditions to engage in their normal activities [10][11][12]. The future wireless body-centric sensing systems enable an infrastructure for remote transfer of sensed physiological data to medical service site for real-time diagnosis and storage in medical database, or to an emergency center where proper actions can be taken [4][8].

Although the vision of pervasive wearable intelligence is compelling, it faces several challenging demands that have prevented it from attaining widespread acceptance. Pervasiveness calls for low-cost and low-power technologies, whereas wearability puts strong demands on seamless integrability. Further, the technology must interface with wireless sensor networks to incorporate embedded intelligence. Among the various technologies that potentially converge to this vision, Radio Frequency Identification (RFID) is one of the most promising candidates [2][13][14][15][16][17][18]. This automatic identification technology uses electrically active tags – low-cost and low-power wireless

communication devices that let themselves transparently and unobstructively be embedded into everyday objects to remotely track and monitor current and historical information of the object's physical location, origin, and ownership. When augmented with various ambient and biochemical sensors, the tag is capable of detecting physical parameters of the environment, such as temperature and humidity [21], and providing continuous monitoring of physiological conditions, making early disease detection and prompt actions to health threats possible [12][17][22]. Tremendous amount of tagged entities would establish an intelligent infrastructure that could convert simple observations into higher-level events that can be used for building end-user applications [2][18]. Moreover, RFID technology is standardized and today there is a wide availability of internet infrastructures providing networked services to complement RFID so that a complete system functionality is achieved.

The seamless integration of wearable tags into daily clothing enables a dense infrastructure for the wireless networking of portable and mobile computing devices, allowing these devices to communicate and interoperate with one another. Indeed, wearable tags in body-centric systems has the huge potential to bring the vision of pervasive wearable intelligence closer to reality. Nonetheless, the emerging wearable body-centric applications introduce new challenges for designers developing efficient and sophisticated RFID systems. Traditional tag design parameters and solutions will no longer respond to the new requirements. Instead, the whole RF community must adopt new methods and unconventional approaches to achieve advanced wearable tags that are highly transparently integrated into our daily life. Even today, Harry Stockman's statement in 1948 about the future of RFID in his revolutionary article "Communication by means of reflected power" [19], is extremely timely;

*"Evidently considerable research and development work has to be done before the remaining basic problems in reflected-power communication are solved, and before the field of useful applications is explored."*

## **1.2 The passive UHF RFID system**

Radio Frequency Identification is a wireless automatic identification technology that utilizes electromagnetic interaction to identify, track, and sense objects marked with electrically active transponders, or tags. The main components of an RFID system include the reader, the reader antenna, and the tag. Most tags are comprised of an antenna and an RFID integrate circuit (IC). The IC stores the tag unique digital identification code and contains the logic needed to establish the communication between the tag and the reader according to the utilized communication protocol. The communication link from the reader to the tag is generally referred as the forward link and the link from the tag to reader is referred as the reverse link. The reader unit is connected to the data management system that stores the data linked to the tag identification code and processes the data for the intended end-application. Ongoing research explore also chipless RFID systems [23]. These systems rely on the frequency-dependent behavior of reflected radio waves from chipless antenna-like strands to identify objects. Such an approach promises an extremely low-cost identification solution, but at the expense of lost logic capabilities and greatly reduced identification ranges.

Depending on the mechanism of electromagnetic interaction, RFID systems can be split into near-field and far-field systems. Near-field systems operate in the low frequency (LF) and high frequency (HF) bands commonly at 125 kHz and 13.56 MHz center frequencies, respectively. In these systems, the operational wavelength is much larger than the antennas and most of the available energy from the reader antenna is confined to a region near the reader antenna and comparable to it in size, and decays rapidly

with distance. The interaction between the reader and the tag is therefore based on inductive coupling and the read range of the tag is limited up to tens of centimeters [23]. Far-field systems operate in the ultra-high frequencies (UHF), ranging from 300 MHz to 3 GHz. The UHF antennas are equal or smaller than the operational wavelength. The UHF RFID systems use propagating electromagnetic waves for communication, which enables substantially longer read ranges compared to near-field RFID systems. The read range of UHF RFID systems ranges from a few meters up to hundreds of meters depending on the tag implementation.

Depending on the implementation of the power supply to the tag, the RFID system can be classified as active or passive. Fully active tags are complete radios, including battery, receiver, transmitter, and control circuitry [23], whereas semi-active tags use their internal battery source to activate the tag IC, but still use the reader antenna power for communication [23][24]. Passive tags have no power source. Instead, they rely solely on the external power harvested from the reader antenna to run their circuitry and for data transmission. The communication between the tag and the reader is asymmetric in the sense that rather than creating its own transmission, the passive tag instead receives all the commands wirelessly from the reader unit and uses backscattered modulation to communicate back to the reader unit. This allows for a relatively complex reader to be used with an extremely simple tag, which may be fabricated at low cost. Furthermore, the absence of a battery eliminates the need for maintenance or battery replacement, which increases the tag life time. At system level, small number of fixed or mobile readers can be used with a dense infrastructure of tags, thus keeping the overall system cost low. This has allowed large-scale commercial applications in the supply chain, ticketing, asset tracking, maintenance, and personal identification [18].

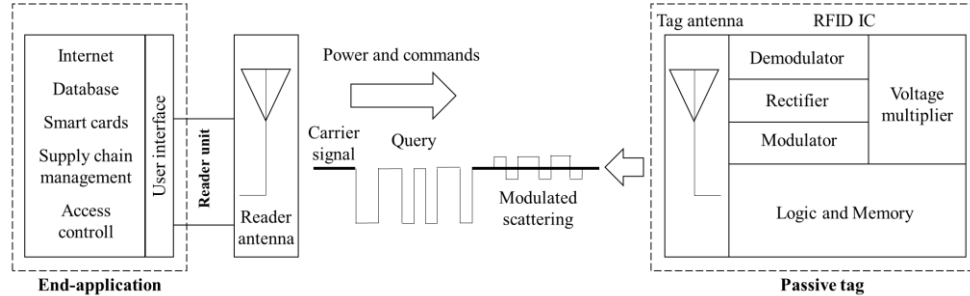


Figure 1. Basic operation principle of a passive backscatter UHF RFID system.

The work presented in this thesis is focused on passive UHF RFID systems operating in the 860–960 MHz band. The system main functional blocks and operation principle are illustrated in Fig. 1. The reader unit generates a high frequency unmodulated carrier signal, which is transformed to a propagating electromagnetic wave by the reader antenna. Once captured by the tag antenna, the electromagnetic wave induces a voltage  $V_a$  across the antenna terminals. When the voltage is high enough, the tag IC internal rectifiers convert the alternating current into a direct current. Voltage multipliers are used to boost the direct voltage to the operating level (sensitivity) of the tag IC. When the tag IC is fully activated, it starts to listen commands from the reader. The reader modulates and encodes the carrier signal to convey the command and ensure that sufficient power is always being transmitted regardless of the data contained within it to the tag. A demodulator on the tag IC extracts the command from carrier signal. If a query-command is received, the reader demands for the tag unique digital identification code,

known as the electronic product code (EPC), stored in the tag IC memory. The tag responds by using the tag IC modulator, which switches the antenna impedance between two states in accordance with the data being sent. This way the requested information is modulated in the scattering from the tag. The reader receiver demodulates and decodes the received tag response, after which the data is transferred to the end-application, for example, data base. The telecommunication protocol utilized by passive UHF RFID systems is standardized under the ISO 18000-6 standard [25]. The tags are standardized under the EPCglobal UHF Class 1 Generation 2 standard [26].

The radio spectrum is divided into geographical sub-bands with regulated equivalent isotropically radiated power (EIRP) limits listed in Table 1. It is defined as the product of the accepted power by the transmitting antenna  $P_t$  and its maximum gain  $G_t$  within the regulated frequency band. This assures the maximum radiated power density for any transmitting antenna. The attainable read range from the passive UHF RFID tag is strongly dependent on the transmitted power used for the power supply to the tag IC. Nonetheless, with the advances in low-power and low-voltage integrated CMOS technologies, the reading sensitivity of commercial tag ICs has dropped to tens of microwatts [27], although sensitivities as low as a couple of microwatts have been presented [28].

Table 1. Regulations for passive UHF RFID systems [26].

Region	Frequency band [MHz]	EIRP = $P_t G_t$ [W]
Europe	865.6–867.6	3.28
United States	902–928	4
Japan*	952–956.4	4
China	840.5–844.5, 920.5–924.5	3.28
Australia	920–926 918–926	4 1

\*Effective until March 21, 2018

Although the market for RFID tags is already well established, the technology is subjected to many challenges which have delayed its global acceptance and ubiquitous use. One major challenge is the development of inexpensive tag fabrication techniques for the economical manufacture of large-scale item-level RFID systems to allow competition against the currently used low-cost bar code systems. Further, the lack of a unified globally interoperated RFID standard due to local regulations makes it problematic to realize the full benefits of RFID applications [29]. The growing interest of wearable passive UHF RFID in biomedical applications puts stringent demands on tag integrability, durability, and reliability. Electromagnetic waves at UHF have the tendency to be absorbed or reflected from objects and materials, making the power and data transfer between the reader and the tag vulnerable to the application environment. Further, various materials, such as liquids and metals, in close vicinity of the tag cause significant changes in the tag antenna parameters, which may have degrading effects on the overall tag performance. This creates challenges in the design of platform-tolerant tags. Here, the impedance matching of the passive tag antenna to the complex and non-linear tag IC is a major issue for the efficient power transfer between the two tag components. Other concerns for pervasive RFID computing are related to privacy and data security [18][30]. Tags are read wirelessly, and typically they do not store history of past readings. They may be read by entities other than their owners and without their owners' awareness. Universal tagging would inevitably involve a tradeoff whereby individuals will be required to give up a proportion of their privacy in exchange for added value [18].

### 1.3 Scope and objectives of the thesis

In this thesis, the focus is on achieving improved design methods and characterization tools for advancing the development of wearable passive UHF RFID tags for wireless body-centric systems requiring light-weight, conformal, and integrable tag antennas. This work is considered as an important milestone in the development towards wearable intelligence and for the industrial developments of garment-integrated RFID tags. It serves to respond to Harry Stockman's request by adding wearable passive RFID technology to the field of useful applications of reflected-power communications and by addressing the technology fundamental problems as follows.

To meet the abovementioned challenges, this study takes an empirical as well as a theoretical approach to achieve highly practical results that are supported by firm theoretical analysis. The scope of this thesis covers the entire design and fabrication procedure for the realization of advanced and novel wearable tag antennas, optimized to achieve excellent RF performance in close vicinity of the human body.

The following steps have been taken to fulfill the objectives of this thesis; the human body effects on wearable passive UHF RFID tag performance is investigated [I][II][i][ii][iii], and a novel approach to model the human body in body centric wireless systems for initiating the design of optimized wearable UHF tags is developed [II][ii][iii]; a technique to optimize the wearable ground plane in passive UHF RFID patch antennas is explored [III]; fundamental UHF characteristics of wearable electro-textiles are established and verified [IV][iv]; applicable methodologies for the characterization of an arbitrary UHF antenna electro-textile and for the optimization of embroidered UHF antenna patterns are proposed [IV]; and an unprecedented fully wearable and flexible embroidered passive UHF RFID patch antenna is fabricated [IV] and analyzed for localization applications [V].

### 1.4 Structure of the thesis

This dissertation is based on five publications, denoted [I]–[V]. The scientific contributions from these publications are discussed and integrated in the introductory part, which is divided into five chapters. The structure of the thesis is illustrated in Fig. 2. This thesis work is also supported by the author's publications [i]–[x]. References are cited with Arabic numbers.

Chapter 1 serves as an orientation to body-centric wireless systems and highlights the motivation and objectives of the thesis. The concepts of pervasive computing and wearable intelligence are discussed. Key features of wearable passive UHF RFID systems are presented. Finally, the scope of this thesis is stated.

Chapter 2 provides the theoretical background and research methodology for the thesis research work. Fundamental antenna theory, important tag antenna parameters and performance indicators, and the scattering principle in passive UHF RFID systems are covered. Further, basic theory of microstrip patch antennas is given. Finally, a modeling methodology for the human body in UHF body-centric systems is proposed.

Chapter 3 concentrates on wearable passive UHF RFID tags. The concept of electro-textiles is detailed. Benefits and challenges of wearable antenna implementation are examined, as well as wearable antenna reliability issues.

Chapter 4 presents established fundamental characteristics of wearable UHF electro-textiles. Benchmarks and design guidelines with innovative optimization methodologies for future novel

wearable antennas are provided. It is evidenced how embroidery techniques can be utilized to achieve wearable tags with extremely high immunity to the human body effects and acceptable read ranges for passive body-centric wireless systems.

Chapter 5 draws the final conclusions and summarizes this thesis's scientific contributions to the state of the art.

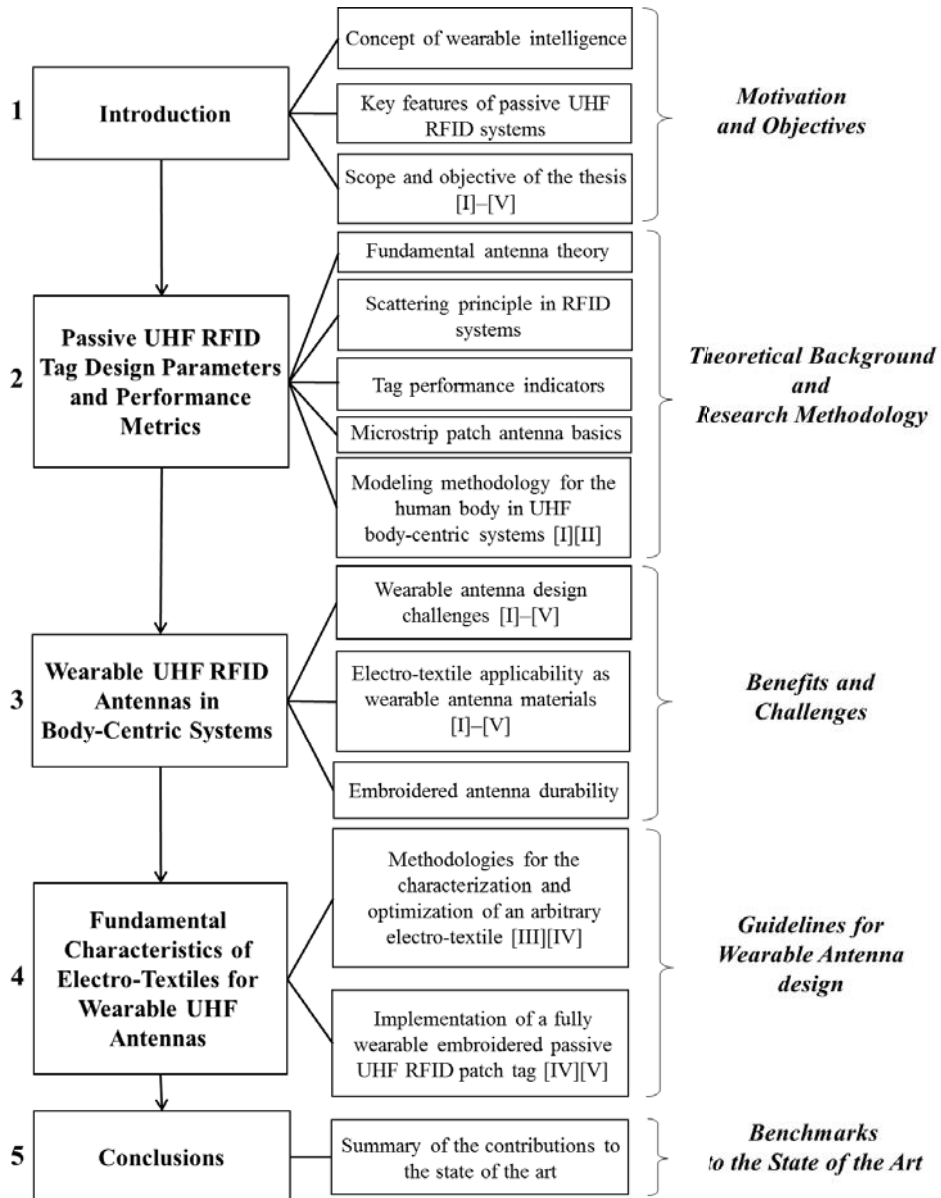


Figure 2. Structure and contents of the thesis.

## 2 PASSIVE UHF RFID TAG DESIGN PARAMETERS AND PERFORMANCE METRICS

The antenna is a central passive structure in any radio system and acts to radiate or receive electromagnetic waves. The propagating electromagnetic wave conveys electromagnetic energy, which enables the power transfer in wireless communication systems. Antenna theory rests heavily on Maxwell's equations, which James Clerk Maxwell presented in 1864 [31].

The antennas for RFID tags are subjected to unique design requirements and constraints. A passive RFID tag has two principal constraints limiting its operation: the available power from the reader antenna and the power transfer efficiency  $\tau$  from the tag antenna to the tag IC. In tag design, this puts the focus on efficient power transfer. The tag IC sensitivity constitutes a critical power level in the overall passive RFID system and determines the maximum achievable operational range of the tag under given power regulations. The power transfer at the tag antenna-IC interface is determined by the impedance matching between these two components. The tag IC impedance is strongly frequency and power dependent. Typically, the tag design starts with specifying the maximum achievable read range with a given tag IC. The antenna layout selection is then based on the requirements for the intended application environment. In general, item-level identification demands cost-effective tags for large-scale manufacturing. This calls for simple and small tags [32].

In many applications, the tag antenna should pose conformal and low-profile characteristics for seamless integration with objects of different shapes and materials. In tag manufacturing, photolithography is widely used to fabricate the conductive antenna components, which are typically made out of copper. Although copper exhibits superior conductivity, it lacks structural integrability. Further, the tag substrate has to withstand the photolithography chemical process, which limits the types of suitable antenna substrates. Another drawback with the process is the creation of great amount of waste and material loss when unwanted metal is removed from the substrate. Additive tag manufacturing methods deposit selectively valuable conductive material onto the substrate material, which result in efficient and cost-effective use of materials. This way, tags can be directly created on a wide variety of substrate materials, which allows the use of novel low-cost and flexible substrates, for example paper [33] and textile based substrates [34]. Conductive textiles, known as *electro-textiles*, allow the seamless and robust integration of RFID tags directly into daily clothing, removing the need for separate antenna substrate [I]-[V][i]-[x][35]. These materials are discussed in detail in chapter 3.

Objects of different materials in close vicinity of the antenna may significantly affect the antenna current distribution and thus the antenna radiation characteristics [36][37][38]. Also the antenna input impedance may be greatly altered, with severe detuning and degraded operational range as a consequence [37][38]. Dissipative materials, such as liquids, convert electromagnetic energy into heat, which yet limits the available power for the tag antenna [38]. Platform tolerance is a challenging tag design requirement. Antennas with ground plane, for example patch and planar inverted-F antennas, provide inherent antenna-matter isolation and are typically favored near dissipative dielectric or metallic materials [39][40][41][42][43] at the expense of more complex structures and higher unit cost compared to one-layer dipole and slot antennas. Traditionally, large ground planes are used in the antenna structures to decrease the effects of the platform on the antenna input impedance and to achieve comparatively high antenna directivities for potentially longer operation ranges [42][43][44]. However, in case of electro-textile ground



planes, other parameters than the electrical size of the ground plane will determine the antenna platform tolerance and the radiation pattern, as verified in chapter 4.

## 2.1 Antenna radiation characteristics

### *Field regions and input impedance*

The electromagnetic field structure varies at different distances  $r$  from the antenna. The space surrounding the antenna may be divided into three regions: reactive near-field, radiating near-field, and far-field. The reactive near-field exists closest to the antenna. In this region, the power flow density vector out of a sphere of radius  $r$  surrounding the antenna has a predominating imaginary component and therefore, there is almost no time-average radial power flow. The imaginary power density corresponds to standing waves, and indicate stored reactive energy. The energy is interchanged between the electric and magnetic field components with time. The radiating near-field exists between the reactive near-field and the far-field. Here, the power flow density vector out of a sphere of radius  $r$  surrounding the antenna has a predominating real component, characterizing radially directed radiated power density, but the angular field distribution is dependent on the distance from the antenna. The far-field region is the region of the antenna field where the angular field distribution is independent on the distance from the antenna. The total complex power flow density out of a sphere of radius  $r$  surrounding the antenna is real-valued and radially directed, indicating in-phase propagating radiation fields. The electric and magnetic field components are perpendicular to each other and transverse to the direction of propagation, forming a transverse electromagnetic (TEM) wave whose field intensity attenuates with the square of the propagation distance in free-space. [31][36] Although the boundaries between the field regions are not consistent, some established criteria are generally adopted to identify the regions. They may be summarized for cases where the maximum dimension  $D$  of the antenna is much larger than the wavelength,  $D \gg \lambda$ , as listed in Table 2. It should be noted, however, that for many UHF tag antennas this assumption is not valid.

Table 2. Field regions for  $D \gg \lambda$  [31][36].

Region	Distance $r$ from antenna
Reactive near-field	0 to $0.62\sqrt{D^3/\lambda}$
Radiating near-field	$0.62\sqrt{D^3/\lambda}$ to $2D^2/\lambda$
Far-field	$2D^2/\lambda$ to $\infty$

The imaginary power density in the near-field is manifested by a reactive component  $X_a$  in the antenna input impedance  $Z_a$ . Although a resonant antenna has a null reactive impedance component, it still has imaginary power density in the near-field. The antenna input impedance is the impedance presented at its input terminals and is defined as the ratio of the voltage to current at the input terminals [36]. The antenna radiates power through the radiation resistance  $R_r$ . Power will also be dissipated in the antenna loss resistance  $R_{ohmic}$  as heat due to ohmic losses on the antenna structure. The antenna current distribution is strongly frequency dependent. Therefore, the antenna input impedance exhibit similar frequency dependence. Consequently, the antenna will be matched to its load only within a limited bandwidth. As discussed previously, the input impedance is affected by nearby objects, but it also depends on other factors, including the antenna geometry and method of excitation [36]. When anisotropic conductive materials are used for the antenna conductor, such as *embroidered textiles*, the textile stitching pattern will constitute a critical factor in the achieved

impedance matching [IV]. This will be clear from chapter 4. Due to the complex behavior of the antenna input impedance, its analytical investigation is in most cases extremely challenging. Fortunately, commercially available electromagnetic solvers are today available that enables antenna simulations.

### **Radiation pattern**

The antenna radiation pattern is a mathematical function or graphical representation of the antenna radiation properties, typically in the far-field, as a function of space coordinates [36]. Usually, the spherical coordinate system centered on the antenna is used. Antennas are reciprocal structures, and hence, the radiation pattern is the same on transmission and reception of electromagnetic waves. The prime radiation property is the two- or three-dimensional spatial distribution of radiated energy as a function of the observation point. A magnitude electric or magnetic *field pattern*,  $|\vec{E}|$  or  $|\vec{H}|$ , respectively, has at each observation point on the surface of a sphere of constant radius  $r$  three electric and magnetic field components:  $(E_r, E_\theta, E_\phi)$  and  $(H_r, H_\theta, H_\phi)$ . In the far-field, the radial field components are vanishingly small compared to either one, or both, of the two other components, and the relationship between the radiation components follows that of a TEM wave [31]

$$\vec{H} = \frac{1}{\eta} \vec{r} \times \vec{E}, \quad (1)$$

where  $\eta$  is the wave impedance of the medium (in vacuum  $\eta \approx 377 \Omega$ ) and  $\vec{r}$  is the direction of propagation. The *power pattern* represents the power density as a function of the angular space. Generally, the field and power patterns are normalized to their maximum values, yielding the normalized field  $F(\theta, \phi)$  and power  $P(\theta, \phi)$  patterns [31]

$$F(\theta, \phi) = \frac{E(\theta, \phi)}{\max(E(\theta, \phi))}, P(\theta, \phi) = |F(\theta, \phi)|^2. \quad (2)$$

Radiation patterns are frequently given in decibels. From the definition in (2) it follows that the normalized field and power patterns are the same in decibels.

An isotropic radiator is a hypothetical lossless antenna that radiates the fields equally in all directions. In practice, the radiation pattern is directional or omnidirectional. A directional antenna emphasizes the radiating energy in some direction and suppresses it in others. An omnidirectional radiation pattern is a special type of directional pattern; it has an essentially non-directional pattern in a given plane and a directional pattern in any orthogonal plane. In practice, the three-dimension radiation pattern is measured as several two-dimensional patterns. In case of a linearly polarized antenna, the E- and H-planes are usually measured to describe the antenna radiation properties. The E-plane contains the electric field vector and the direction of maximum radiation, whereas the H-plane contains the magnetic field vector and the direction of maximum radiation. [36]

### **Directivity**

The directivity  $D(\theta, \phi)$  is defined as the ratio of the radiation intensity in one direction  $(\theta, \phi)$  to the average radiation intensity [31][36]. The radiation intensity  $U(\theta, \phi)$  is the power radiated in a given direction per unit solid angle, measured in watts per steradians or square radians [31]

$$U(\theta, \phi) = \left( \text{Re} \vec{S} \cdot \vec{r} \right)^2 = S(\theta, \phi) r^2 = U_{\max} |F(\theta, \phi)|^2, \quad (3)$$

where  $\vec{s}$  is the Poynting vector describing the power density of the radiation,  $U_{\max}$  is the maximum radiation intensity, and  $|F(\theta, \phi)|^2$  is the linear power pattern normalized to a maximum value of 1 in the direction of maximum radiation intensity. For a non-isotropic source in the spherical coordinate system, the average power intensity per steradians can be defined as [31]

$$U_{ave} = \frac{1}{4\pi} \int_0^{2\pi} \int_0^\pi U(\theta, \phi) \sin\theta d\theta d\phi = \frac{P_{rad}}{4\pi}. \quad (4)$$

This average power intensity equals the radiation intensity  $U(\theta, \phi)$  that an isotropic source with the same input power  $P_{rad}$  would radiate. Substitution of (3) and (4) in definition of the directivity yields

$$D(\theta, \phi) = \frac{U(\theta, \phi)}{U_{ave}} = \frac{|F(\theta, \phi)|^2}{\frac{1}{4\pi} \int_0^{2\pi} \int_0^\pi |F(\theta, \phi)|^2 \sin\theta d\theta d\phi}. \quad (5)$$

From (5) it is clear that the directivity is dimensionless and solely determined by the pattern shape.

### **Efficiency**

The directivity of the antenna assumes that the antenna is lossless and that all accepted input power appears as radiated power:  $P_{in} = P_{rad}$ . In practice, some of the accepted input power is absorbed on the antennas as ohmic losses  $P_{ohmic}$  (conduction and dielectric losses), and does not appear as radiated power. The *antenna radiation efficiency*  $e_{cd}$  takes this into consideration [31][36]

$$e_{cd} = \frac{P_{rad}}{P_{in}} = \frac{P_{rad}}{P_{rad} + P_{ohmic}} = \frac{R_r}{R_a} = \frac{R_r}{R_r + R_{ohmic}}, 0 \leq e_{cd} \leq 1. \quad (6)$$

The *antenna gain* describes how efficiently the antenna transforms available power at its input terminals to radiated power together with its directive properties compared to a hypothetical isotropic antenna ( $e_{cd} = 1$  and  $D(\theta, \phi) = 1$ ) [31]

$$G(\theta, \phi) = e_{cd} \frac{U(\theta, \phi)}{U_{ave}} = e_{cd} \frac{4\pi U(\theta, \phi)}{P_{rad}} = e_{cd} D(\theta, \phi). \quad (7)$$

The losses due to mismatching between the antenna input terminals and the antenna feed line are counted for in the reflection or mismatch efficiency  $e_r$ . The total antenna efficiency can now be written as [36]

$$e_{tot} = e_{cd}(1 - |\Gamma|^2) = e_{cd}e_r, \Gamma = \frac{Z_a - Z_0}{Z_a + Z_0}, \quad (8)$$

where  $Z_0$  is the characteristic impedance of the feed line.

## **2.2 Tag antenna impedance matching and antenna scattering**

### **Impedance matching**

The RFID tag antenna is directly matched to the complex tag IC impedance. A proper impedance matching assures efficient power transfer between the tag antenna and the tag IC, and hence, it enables long operation ranges. The power transfer efficiency may be investigated by analyzing a one port network, shown in Fig. 3, representing a generator (antenna with source phasor magnitude voltage  $|V_a|$ )–load (tag IC) circuit with

complex source and load impedances,  $Z_a$  and  $Z_{ic} = R_{ic} + jX_{ic}$ , respectively. The impedance  $Z_{ic}$  is assumed to be the tag IC input impedance at the IC sensitivity level.

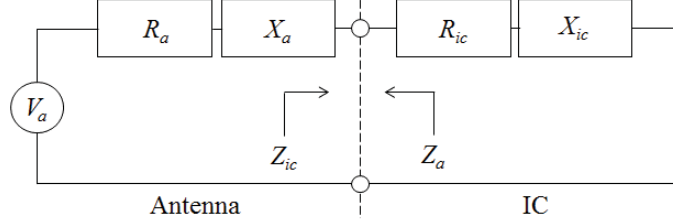


Figure 3. Thévenin equivalent circuit of a passive RFID tag.

In Fig. 3, the time-average power dissipated in the tag IC is given by Ohm's law as

$$P_{ic,av} = I_{rms}^2 R_{ic} = \frac{1}{2} |I|^2 R_{ic} = \frac{1}{2} \left( \frac{|V_a|}{|Z_a + Z_{ic}|} \right)^2 R_{ic}, \quad (9)$$

where  $|I|$  is the phasor magnitude current in the circuit. The power delivered to the tag IC is maximized under conjugate matching [23], so that  $Z_a = Z_{ic}^*$ , where the star indicates complex conjugate. The power transfer at the antenna–IC interface is written using (9) such that

$$\tau = \frac{P_{ic,av}}{P_{ic,av}|_{\max}} = \frac{4R_a R_{ic}}{|Z_a + Z_{ic}|^2} = 1 - |\Gamma^*|^2, \Gamma^* = \frac{Z_{ic} - Z_a^*}{Z_{ic} + Z_a}, \quad (10)$$

where  $\Gamma^*$  is power wave reflection coefficient [45] describing the mismatch between the tag antenna and the tag IC. Since the tag IC input impedance is inherently capacitive [46][47], the input reactance of the tag antenna input impedance must provide a corresponding inductive component for maximum power transfer between the IC and the tag antenna.

The antenna self-resonance frequency  $f_0$  occurs at the lowest frequency for which the antenna input reactance equals zero. The antenna input impedance characteristics below self-resonance is different for different antenna types. For small dipoles, the tag antenna input reactance is capacitive below  $f_0$ , and consequently, matching techniques needs to be considered for efficient power transfer. In general, the tag antenna structure itself is modified to provide the required inductive component in the input reactance by introducing, for example, inductive loops or sections of meander lines arrangements [48][II]. Depending on the design choice, the input reactance for a microstrip patch antenna can be inductive below  $f_0$  [III][36]. Nevertheless, matching networks are typically incorporated to optimize the power transfer at desired operational frequency. The antenna may be sourced via an inductively coupled small loop placed in close vicinity to the radiating body. The loop adds simultaneously an equivalent inductive component in the tag antenna input impedance [48][49]. Another matching configuration incorporates inductive shorting strips [50][III].

### Scattering principle

In passive UHF RFID systems, the tags reply to the reader by emitting *modulated scattering* while illuminated by the reader antenna carrier wave. The radar cross section (RCS)  $\sigma$  is usually used to describe

the scattered power density  $S_{scat}$  at a distance  $r$  from a target when an incident power density  $S_{inc}$  impinges on it [23][31][36][51][52][53]

$$\sigma = 4\pi r^2 \frac{S_{scat}(\theta, \phi)}{S_{inc}(\theta_{inc}, \phi_{inc})}. \quad (11)$$

For RFID tags, the differential RCS  $\Delta\sigma_r$  is commonly used to determine the power of the modulated signal backscattered to the reader [52][54]. It is function of the tag antenna gain and the matching between the tag antenna and the two modulating states, absorbing or reflecting, of the tag IC impedance.

The average power density of an electromagnetic wave incident to the tag antenna at a distance  $r$  from the reader antenna with a gain  $G_t$  is attained using (3) and (4) as

$$S_t(\theta, \phi, r) = \frac{P_t G_t(\theta, \phi)}{4\pi r^2}. \quad (12)$$

The receiving tag antenna acts to convert incident power flux  $S_{t,inc}$  to power delivered to the load. The power available for the antenna load under conjugate matching condition is given by the antenna maximum effective aperture  $A_{e,r,max}$  [23][51]

$$P_{r,max} = S_{t,inc}(\theta_{inc}, \phi_{inc}) A_{e,r,max}. \quad (13)$$

Antenna ohmic losses  $R_{ohmic}$  are included in  $A_{e,r,max}$ . Losses that are not inherent for the antenna, but depend on how the tag antenna is used in the communication system, are not included. These include polarization losses and impedance mismatch losses. The polarization loss factor  $\chi_{pol}$  is given by the relative alignment of the electric field polarization vectors of the tag antenna and the incident wave,  $\hat{\rho}_a$  and  $\hat{\rho}_w$ , respectively [36]. Taking these losses into account and expressing the effective aperture with use of the tag antenna gain  $G_r$  [23][51] the available power for the tag antenna load is attained as

$$P_r = S_{t,inc}(\theta_{inc}, \phi_{inc}) A_{e,r,max} \chi_{pol} \left(1 - |\Gamma^*|^2\right) = S_{t,inc}(\theta_{inc}, \phi_{inc}) \frac{\lambda^2}{4\pi} G_r(\theta_{inc}, \phi_{inc}) \chi_{pol} \left(1 - |\Gamma^*|^2\right). \quad (14)$$

In general, the total scattered power from a loaded antenna is composed of two components: the structural mode and the antenna mode [36][51][54]. The structural mode is related to the surface currents induced on the antenna even if the antenna is terminated according to the conjugate matching principle. The structural mode is equivalent with scattering of general targets, and is determined by the antenna structure, shape, and material [36][51]. The antenna mode scattering originates from the energy absorbed by the antenna load of a lossless antenna as well as from the power reflected at the antenna-IC interface [31]. It is completely determined by the radiation properties of the antenna and the pattern of the energy scattered is identical to that of the antenna radiation pattern [31]. The surface currents induced due to structural mode scattering are not flowing through the antenna input terminals and hence, this mode is not affected by the tag impedance modulation. As a result, the backscattered power from the tag is assumed to only originate from the antenna mode scattering [23][54]. The backscattered power is the total power re-radiated  $P_{re-rad}$  from the tag antenna, which under given assumptions equals to the available power for the tag antenna that is not delivered to the load but reflected from the load. Using (12) and (13) the power density of the antenna mode scattered field is

$$S_{scat}(\theta, \phi, r) = \frac{P_{re-rad} G_r(\theta, \phi)}{4\pi r^2} = \frac{S_{t,inc}(\theta_{inc}, \phi_{inc}) \frac{\lambda^2}{4\pi} G_r(\theta_{inc}, \phi_{inc}) \chi_{pol} |\Gamma^*|^2 G_r(\theta, \phi)}{4\pi r^2}, \quad (15)$$

$$S_{scat}(\theta, \phi, r) = S_{t,inc}(\theta_{inc}, \phi_{inc}) \frac{\lambda^2}{(4\pi)^2} G_r(\theta_{inc}, \phi_{inc}) \chi_{pol} |\Gamma^*|^2 G_r(\theta, \phi).$$

The RCS of the tag antenna  $\sigma_r$  is written using (11) and (15) as

$$\sigma_r = \frac{\lambda^2}{4\pi} G_r(\theta_{inc}, \phi_{inc}) \chi_{pol} G_r(\theta, \phi) |\Gamma^*|^2. \quad (16)$$

The RFID tag IC modulates the tag antenna RCS through load modulation by changing its impedance between two states. This way, the magnitude and phase of the received signal by the reader changes, allowing data exchange between the reader and the tag. The differential or modulated tag antenna radar cross section is [52]

$$\Delta\sigma_r = \frac{\lambda^2}{4\pi} G_r(\theta_{inc}, \phi_{inc}) \chi_{pol} G_r(\theta, \phi) K, \quad K = \alpha |\Gamma_1^* - \Gamma_2^*|^2, \quad (17)$$

where  $K$  is the modulation loss factor,  $\Gamma_1^*$  and  $\Gamma_2^*$  are the power wave reflection coefficients corresponding to the two RFID IC impedance states, and  $\alpha$  accounts for the used modulation scheme effects.

### 2.3 Performance indicators

Measurements of small RFID tag antennas is challenging because the feed line to the antenna input port is difficult to obtain. Further, a feed line measurement lacks accuracy as the feed line couples strongly to the antenna and radiates as part of the antenna [55]. Although baluns provide means to reduce the cable-related effects [56][57], measurement instruments near the antenna may alter the antenna characteristics. A more convenient approach is to use wireless measurement techniques for the performance evaluation of fully assembled tags [I]–[V], which simultaneously accounts for the tag IC mounting parasitics.

One fundamental tag parameter is the *realized tag antenna gain*  $G_{r,real}$ . It takes into account the antenna–IC impedance matching compared to perfectly matched isotropic tag antenna and is given by

$$G_{r,real}(\theta, \phi) = \tau G_r(\theta, \phi) = \tau_{cd} D_r(\theta, \phi). \quad (18)$$

The *tag antenna normalized power pattern*  $P_r(\theta, \phi)$  is attained by normalizing  $G_{r,real}(\theta, \phi)$  to its maximum value  $G_{r,max}$  over the desired spatial angles for a given frequency.

In most cases, the *tag maximum read range* is considered as the ultimate tag performance indicator that determines the tag applicability in the specific application environment [52][58]. This is the longest range the reader is able to detect the backscattered power from the tag under given power regulations. The maximum read range is highly application dependent as materials in close vicinity of the tag will affect the tag antenna radiation characteristics and the backscattered power from the tag will interact with obstacles between the reader and tag antennas. From maximum read range point of view, comparison of tags is hence only convenient when a reference environment is defined. When defined as free-space, Friis' transmission equation [36] may be used to estimate the maximum tag read range. In this case, the read range is referred

as the *tag maximum theoretical read range*  $r_{\max}$ . In free-space, the available power for the tag IC under given power regulations is attained by (14) and (18) as

$$P_r(r) = S_{t,inc}(\theta_{inc}, \phi_{inc}) \frac{\lambda^2}{4\pi} \chi_{pol} G_r(\theta_{inc}, \phi_{inc}) \left(1 - |\Gamma^*|^2\right) = \frac{EIRP}{4\pi^2} \frac{\lambda^2}{4\pi} \chi_{pol} G_{r,real}(\theta, \phi). \quad (19)$$

The EIRP value is defined for the maximum transmitter antenna gain  $G_{t,max}(\theta_{\max}, \phi_{\max})$ . For passive UHF RFID tags, the sensitivity of the RFID IC is typically the achievable read range limiting factor. The tag maximum theoretical read range is with this assumption attained for the case when the received tag IC power equals the sensitivity of the tag IC, that is  $P_r(r) = P_{ic,th}$ . From (19) this yields the forward link read range

$$r_{\max}(\theta, \phi) = \frac{\lambda}{4\pi} \sqrt{\frac{G_{r,real}(\theta, \phi) \chi_{pol} EIRP}{P_{ic,th}}}. \quad (20)$$

Clearly, maximization of the tag antenna gain and optimization of the impedance matching at the tag antenna–IC interface are crucial factors for maximized tag read range.

In practice, to attain measureable and comparable read range results, that at the same time are comparable with the simulation results of an isolated tag, an artificial free-space environment may be used. The anechoic chamber is such an environment. As the chamber is often restricted in size, it is advantageous to measure the tag maximum read range with fixed distance  $d$  between the reader and tag antennas. This is possible when utilizing a ramping down method of the reader transmitted power. While the reader is communicating with the tag, the reader transmitted power is decreased at every frequency point considered until  $P_r(r) < P_{ic,th}$ . This is the threshold power  $P_{th,min}(\theta, \phi)$  of the tag, or equivalently, the reader minimum threshold power for successful communication with the tag at a distance  $d$  away from the reader antenna. The ramping down method can be realized with an RFID reader with adjustable output power and transmission frequency. The Voyantic Tagformance measurement system [59], was used in [I]–[V] to characterize the tags. The system enables channel characterization, after which the measured read range become independent on the used measurement set-up and on the distance  $d$ . The channel is characterized by utilizing the system calibration tag to measure the link loss factor  $L_{iso}$ , which is defined from the reader output port to the input of a hypothetical polarization-matched isotropic antenna located at a distance  $d$  away from the reader antenna. Using the measured quantity  $L_{iso}$  in (19) yields

$$P_{ic,th} = P_{th,min}(\theta, \phi) L_{iso} \chi_{pol} G_{r,real}(\theta, \phi) \Rightarrow G_{r,real}(\theta, \phi) = \frac{P_{ic,th}}{\chi_{pol} L_{iso} P_{th,min}(\theta, \phi)}. \quad (21)$$

Substituting  $G_{r,real}(\theta, \phi)$  in (20) into (20) gives the measured theoretical tag read range as

$$r_{\max}^m(P_{th,min}(\theta, \phi)) = \frac{\lambda}{4\pi} \sqrt{\frac{EIRP}{L_{iso} P_{th,min}(\theta, \phi)}}. \quad (22)$$

The threshold power-on-tag describes the minimum amount of power at the tag terminals to activate the tag IC and can be written as

$$P_{on-tag,th} = P_{th,min} L_{iso}. \quad (23)$$

The measured link loss factor follows from (23) as

$$L_{iso} = \Lambda / P_{th,\min}^* \quad (24)$$

where  $\Lambda$  is a known constant describing the sensitivity of the calibration tag and  $P_{th,\min}^*$  is the measured threshold power of the calibration tag during channel characterization. The measured quantities in (22) are thus  $P_{th,\min}^*$  and  $P_{th,\min}(\theta, \phi)$ .

The tag antenna measured normalized power patterns are attained by utilizing (21) and (24) as follows

$$P_r^m(\theta, \phi) = \frac{G_{r,real}(\theta, \phi)}{G_{r,max}} = \frac{k / P_{th,\min}(\theta, \phi)}{k / \min(P_{th,\min}(\theta, \phi))} = \frac{\min(P_{th,\min}(\theta, \phi))}{P_{th,\min}(\theta, \phi)}, k = \frac{P_{ic,th}}{\Lambda / P_{th,\min}^*}. \quad (25)$$

In summary, all tag performance indicators are calculated from measured threshold powers levels.

## 2.4 Microstrip patch antenna

Microstrip patch antenna configurations are common design choices for enhanced platform tolerance [39][40][41][42][43]. As seen in Fig. 4, a microstrip antenna in its simplest configuration consist of a radiating patch of  $L$  in length and  $W$  in width on a dielectric substrate material having a thickness  $h$  and a ground plane on the other side.

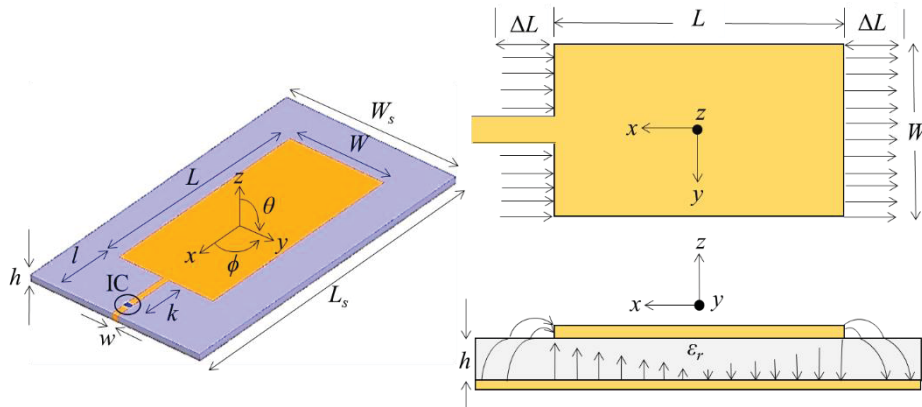


Figure 4. Passive RFID patch tag antenna.

The height  $h$  is typically much smaller than the wavelength, usually between  $0.003\lambda_0$  and  $0.05\lambda_0$ , where  $\lambda_0$  is the wavelength in free-space. For good radiation efficiencies, the length  $L$  is typically between  $\lambda_0/3$  and  $\lambda_0/2$  [36]. However, the overall size of the patch antenna is larger due to the demand of a ground plane that is larger than the radiating patch to accommodate the fringing of the electric fields at the edges of the patch [60]. The fringing fields are responsible for the radiation.

The region between the patch antenna conductors may be modeled as an open ended transmission-line [31][36][43]. The electric field lines in Fig. 4 are perpendicular to the conductors according to the boundary conditions [36], and resembles those of a static case. The amount of fringing is dependent on the dimensions of the patch and the substrate height. For the E-plane ( $xz$ -plane) the fringing is a function of the ratio  $L/h$



and the value of the substrate dielectric constant  $\epsilon_r$ . As  $W/h \gg 1$  and  $\epsilon_r > 1$ , most of the field is confined in the substrate. The fringing acts to extend the effective length  $L_{eff}$  of the patch. This extension is represented by two radiating slots of length  $\Delta L$  in Fig. 4. In the half-wavelength patch, the field varies one  $\lambda_{eff}/2$  cycle along the length of the patch, where  $\lambda_{eff}$  is the effective wavelength  $\lambda_{eff} = \lambda_0 / \sqrt{\epsilon_{r,eff}}$ , and  $\epsilon_{r,eff}$  is the effective dielectric constant. There is no field variation along the width of the patch. Along the width of the patch the voltage is maximum and current is minimum due to open end. The formed standing wave in the substrate leads to electric fields that are of opposite phase on the left and right halves, resulting in total fringing fields at the edges that are of opposite phase but equal in magnitude. However, in the horizontal direction ( $x$ ), the fringing fields are in phase and combine to a broadside radiation pattern, that is, the maximum radiation is towards  $+z$ -direction. Therefore, the patch has two radiating slots with constant electric fields in the same plane as the patch. Fields along other edges of the patch have odd symmetry and the associated radiation cancel in broadside direction. As a result, the patch radiates along its width and its radiation pattern is linearly polarized parallel to the electric fields in the slots ( $xz$ -plane). The length of the radiating slots is a function of the  $W/h$  ratio and the value of  $\epsilon_{r,eff}$ , and may be taken to be equal to the substrate height [31], which is typically a few millimeters in the UHF range. Initial values for the length and width of a resonant half-wavelength patch resonating at a center frequency of  $f_0$  are calculated by neglecting the fringing effect as [36][43]

$$\begin{aligned} L &\approx \lambda_d / 2 = \lambda_0 / (2\sqrt{\epsilon_r}) = c / (2f_0\sqrt{\epsilon_r}), \\ W &\approx \frac{c}{2f_0} \sqrt{\frac{2}{\epsilon_r + 1}}, \end{aligned} \quad (26)$$

where  $c$  is the velocity of light in free-space. The width of the patch antenna has significant effect on the patch antenna input impedance and gain [36][43]. However, the input impedance of the patch antenna can also be tuned by controlling the length  $l$  and width  $w$  of the microstrip-line feed [III][IV]. Inset feeding [36] provides additional impedance tuning parameters, while keeping the overall size of the antenna under control [V].

The patch antenna quality factor  $Q$ , bandwidth BW, and radiation efficiency  $e_{cd}$  are interrelated and when considering the antenna performance, there is always a trade-off between them [61]. The total quality factor  $Q_t$  of an antenna is determined by the overall antenna losses, including radiation, ohmic, dielectric, and surface wave losses. For good conductors on thin ( $h \ll \lambda_0$ ) low-loss antenna dielectric substrates, the total quality factor is usually dominated by the quality factor of the radiation term, which is inversely proportional to  $h$ . For such case, the quality factor is generally high [61]. The fractional bandwidth of the antenna is inversely proportional to the  $Q_t$  [61][43]

$$BW = \frac{\Delta f}{f_0} \sim \frac{1}{Q_t}, \quad (27)$$

where  $\Delta f = f_1 - f_2$ , and  $f_1$  and  $f_2$  are the upper and lower frequencies, respectively, of acceptable antenna performance. These frequencies typically correspond to antenna reflection coefficients of  $-10$  dB. The traditional microstrip antenna poses generally narrow bandwidth [62]. In practice, this means that the antenna input impedance is sensitive to small changes in frequency. The radiation efficiency of the antenna is proportional to the quality factor [62]. For good antenna performance, a thick substrate with low  $\epsilon_r$  and dielectric loss  $\tan \delta$  values is desirable because it provides better efficiency, larger bandwidth, loosely bound fields for radiation into space, but at the expense of larger size [31][36][43]. The bandwidth of the microstrip

patch antenna is directly proportional to  $h$  and inversely proportional to the square root of  $\epsilon_r$  [36][43]. However, as  $h$  increase, excitation of surface waves increase, which reduces the efficiency of the antenna [36][43].

The narrow bandwidth of the traditional patch antenna is often considered as its major drawback [62], preventing its use in many microwave applications. Therefore, novel designs and techniques have been developed for improving the bandwidth of microstrip antennas, of which the double-tuning effect is widely exploited [42][44][62]. In some applications, however, a narrow antenna bandwidth and a high antenna quality factor are desired.

In [III], a reference copper patch tag antenna was designed for the purpose of characterization of wearable antenna materials in the UHF RFID band. The overall design goal was to achieve high tag antenna realized gain  $G_{r,real}$  at 900 MHz together with a high antenna quality factor  $Q_t$ . This assures that the antenna input impedance becomes sensitive to small frequency changes. Based on the general microstrip antenna characteristics, the 3.175-mm thick Rogers RT/Duroid 5880 substrate with the accurately specified dielectric properties  $\epsilon_r = 2.2$  and  $\tan \delta = 0.0009$  was considered as a suitable antenna platform for the reference tag antenna. The used NXP RFID IC has a sensitivity of  $-18$  dBm [27]. The IC on strap has an equivalent input parallel resistance and capacitance of  $2.85 \Omega$  and  $0.9$  pF, respectively [46]. At 900 MHz, the IC impedance is  $Z_{ic} = 13 - j193 \Omega$ . The initial length  $L$  of the patch was calculated from (26). The antenna was simulated using the commercial full-wave electromagnetic solver HFSS from ANSYS [63]. The width  $W$  of the patch was tuned to assure a high radiation efficiency. The length  $l$  and width  $w$  of the feed were adjusted to achieve the required inductive antenna input reactance for efficient antenna to tag IC power transfer. The size of the ground plane was set large enough to attain high antenna directivity. The dimensions of the optimized reference patch tag antenna are summarized in Table 3. A soldered copper shorting strip was used to connect the NXP IC to the ground plane.

Table 3. Reference patch tag antenna optimized dimensions.

Parameter	$L$	$W$	$l$	$k$	$w$	$L_s$	$W_s$
Size [mm]	100	50	30	21	3	150	90

The NXP IC is attached over the 2-mm gap using conductive epoxy resin

The simulated and measured tag realized gains according to (18) and (21), respectively, together with the tag antenna normalized power patterns attained from (25), are presented in Fig. 5. The simulated radiation efficiency and gain at 900 MHz were 97% and 6 dBi, respectively.

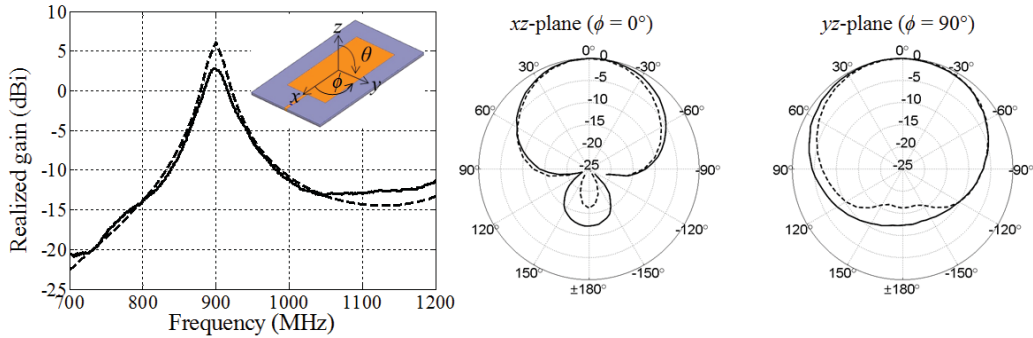


Figure 5. Measured (solid line) and simulated (dashed line) reference patch tag realized gain in  $+z$ -direction and tag antenna normalized power patterns at 900 MHz for the E-plane ( $xz$ -plane) and H-plane ( $yz$ -plane).

As desired, at 900 MHz the reference patch tag poses high realized gain and a high quality factor. The measured tag theoretical read range calculated from (22) with the maximum gain of the reader antenna pointed towards the tag  $+z$ -direction was 17 m at 900 MHz. Although the reference patch tag performance fulfills the requirements of wearable applications, its stiff and bulky substrate prevents it from adapting to such applications. To overcome this constraint, both the conductor and substrate materials are to be replaced by flexible and light-weight ones that enables easy integration with clothing, but without impairing the tag characteristics beyond deficient operation. The studied electro-textiles [I]–[V] provide compelling means for meeting these requirements. Nevertheless, these materials face unique challenges that requires novel solutions for their applicability in wearable applications to become reality. Once all of these challenges are addressed, they will have the enormous potential to revolutionize the wearable intelligence.

## 2.5 Modeling methodology for the human body in UHF body-centric systems

In body-centric systems, the wearable antennas are operated in close vicinity of the human body. In the UHF RFID band, the human body represents a highly dissipative dielectric body. The fields from the radiating wearable antenna tend to couple with the body, which may have serious implications for the antenna performance. The dipole antenna is typical choice for UHF RFID applications thanks to its relatively simple single-layered geometry with well-known impedance matching and miniaturization techniques [48]. Further, they enable easy integration with garments. Unfortunately, in case of an omnidirectional radiator, such as a dipole antenna, the amount of coupling depends greatly on the antenna to body separation  $h$  [ii][37][39][35], as evidenced in Fig. 6. Although high-permittivity materials have been exploited for antenna miniaturization purposes [32][64], the human body cannot be considered as a favorable antenna platform due to its high dielectric losses. In fact, achieving tag read ranges over 2 meters without any isolation layers between the human body and the antenna is challenging [i][ii].

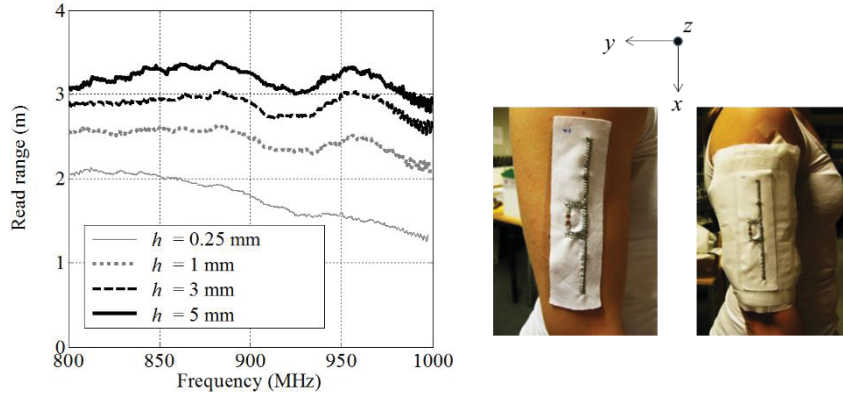


Figure 6. Measured passive UHF RFID dipole tag read range in  $+z$ -direction according to (22) for different antenna to body separations  $h$ . One fabric layer is 0.25 mm thick. [ii]

Sometimes the human body is considered as a reflector as the effects from the body are similar to those from metallic platforms [65][66]. The propagation of an electromagnetic wave relies on the properties of its medium. For a dielectric medium, the wave impedance is proportional to the inverse of square root of  $\epsilon_r$  [31]. The wave impedance of the human body is hence smaller compared to that of free-space. As a result, the propagating wave in free-space will be partly reflected and partly transmitted when incident on the human body. Due to the high dielectric losses, the transmitted wave is rapidly attenuated and is not able to penetrate the human body. This calls for careful selection of the tag location on the human body to minimize shadowing effects and excessive power dissipation [II][35]. Obviously, a single wearable antenna is not enough to assure an omnidirectional radio link, but several antennas distributed over the body are required [II][i][35][67]. For an omnidirectional radiator, the reflective properties of the human body are devastating due to the induced virtual source on the body surface with virtual currents that may have opposite phase than the real antenna source if it is aligned parallel to the body surface [23][36]. Consequently, the antenna radiated field is partially cancelled by the virtual radiation, impairing the antenna radiation efficiency.

The tag performance is not only influenced by the chosen tag location on the human body, but also on the tissue properties. To gain better insight into the effects of different body locations and tissue properties, a copper dipole tag antenna (Fig. 7) was designed for the purpose of on-body measurements [II]. The antenna was implemented on 0.126-mm thick Kapton HN polyimide film ( $\epsilon_r = 3.5$  and  $\tan \delta = 0.0026$ ). Using ANSYS HFSS with the NXP RFID IC equivalent circuit model, the overall goal in the free-space optimization was to achieve a high tag antenna realized gain at the upper UHF RFID band to assure a valid tag on-body response. The optimized tag antenna dimensions are collected in Table 4.

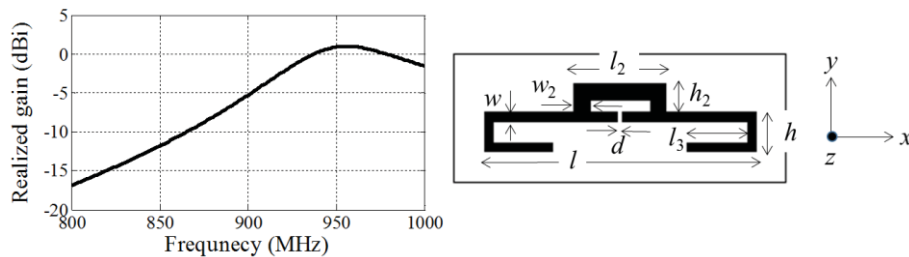


Figure 7. Simulated free-space realized gain in  $+z$ -direction for the dipole tag on Kapton platform.

Table 4. Dipole tag antenna optimized dimensions.

Parameter	$d$	$l$	$l_2$	$l_3$	$w$	$w_2$	$h$	$h_2$
Size [mm]	2	90	30	20	3	5	13	9

The NXP IC is attached over the 2-mm gap  $d$  using conductive epoxy resin

The overall size of the dipole tag was kept small enough to be accommodated on different body locations by folding the two antenna arms. The dipole is equipped with a T-matching loop (parameters  $l_2$ ,  $h_2$ , and  $w_2$ ) that transforms the capacitive tag antenna input reactance component into inductive one. The loop dimensions were optimized to achieve proper antenna-IC impedance matching, and the lengths  $l$  and  $l_3$  were tuned to set the antenna resonance frequency to 950 MHz. The simulated dipole tag realized gain is shown in Fig. 7. The measured read range in  $+z$ -direction in free-space according to (22) at 950 MHz was 10 meters.

The dipole tag read range in  $+z$ -direction was measured in room-sized anechoic chamber environment utilizing the ramping down method of the reader transmitted power on three different body locations and two test subjects. No additional spacers between the tag and the skin tissue were used. The read range was calculated from (22). The overall effects of the human body on the tag performance are embedded in the measured quantity  $P_{th,min}$ . Figure 8 shows the average ranges based on 20 repeated  $P_{th,min}$  measurements. The dissipative human body lowers the antenna quality factor significantly. The introduced losses result in higher recorded  $P_{th,min}$ , which is seen as a degradation in the calculated read range. A small shift in the resonance frequency towards lower frequencies is observed. The standard deviations based on the repeated measurements for the different case studies were low, implying that the measurement dynamic uncertainty was low [II].

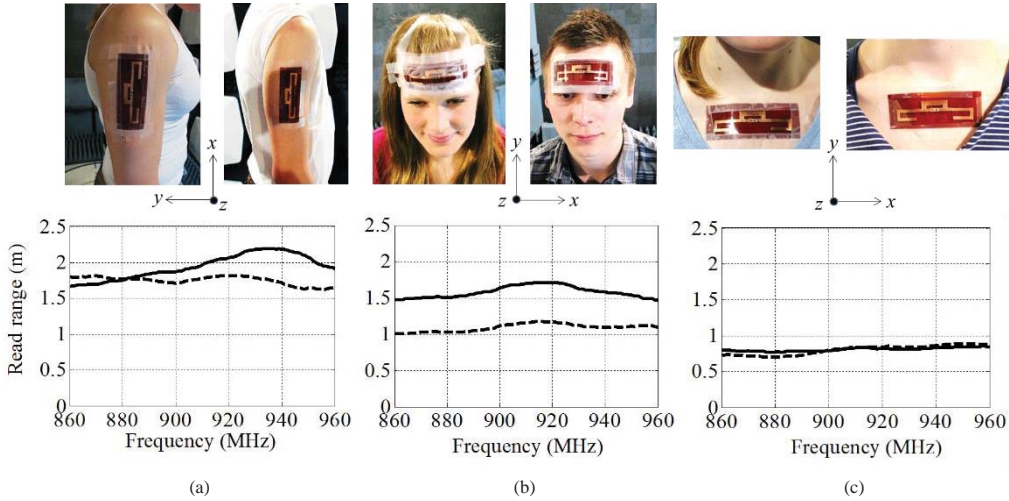


Figure 8. Dipole tag measured on-body read range in  $+z$ -direction for female (solid line) and male (dashed line) for; (a) upper arm, H-plane ( $yz$ -plane); (b) head, E-plane ( $xz$ -plane); and (c) chest, E-plane ( $xz$ -plane).

As the penetration depth inside the human body is small, only the outermost tissue layers, including skin, fat, and muscle tissues, will affect the tag performance, whereas the effects of deeper tissues can be neglected. Another factor affecting the tag response is the degree of the curvature of the considered body

location [68][69][70]. From Fig. 8 it can be observed that the more flat the body surface is, the more prominent will the antenna to body interaction be. For flat surfaces, the tag allows itself to be tightly attached to the skin, whereas for curved surfaces, the antenna to body separation is increased. In fact, the same phenomenon was observed in Fig. 6.

Indeed, the antenna to body interaction is a complex and clearly, a highly case specific mechanism. This was the motivation behind the generation of an application and case specific human body model in [II]. Key requirements for the human body model generation were to; (1) eliminate the need of a database of measured electrical parameters from tissue samples, which to date has played a central role in the developed human body models [65][71][72], and to; (2) establish a modeling methodology that can be easily and quickly adopted in practice to allow one to create an average statistical catalog of human body models for various scenarios. Creation of such a catalog provides a practical, fast, and acceptably accurate engineering tool for initiating the design of wearable UHF RFID tags in body-centric systems.

The flow chart for the developed modeling methodology of the human body is shown in Fig. 9. The model relies on measured on-body threshold response  $P_{th,min}$  from a reference tag of well-known characteristics. This reference response includes not only the effects of the human tissues, but also polarization losses due to imperfect alignment of the tag, and effects of unknown antenna to body separation. The latter effects arise because the reference tag does not allow itself to be perfectly attached to the skin tissue. The mentioned effects are easily overlooked, or even omitted, when small and simplified phantoms are used for the measurement purpose. The measured threshold power is transformed to any desired tag performance metric.

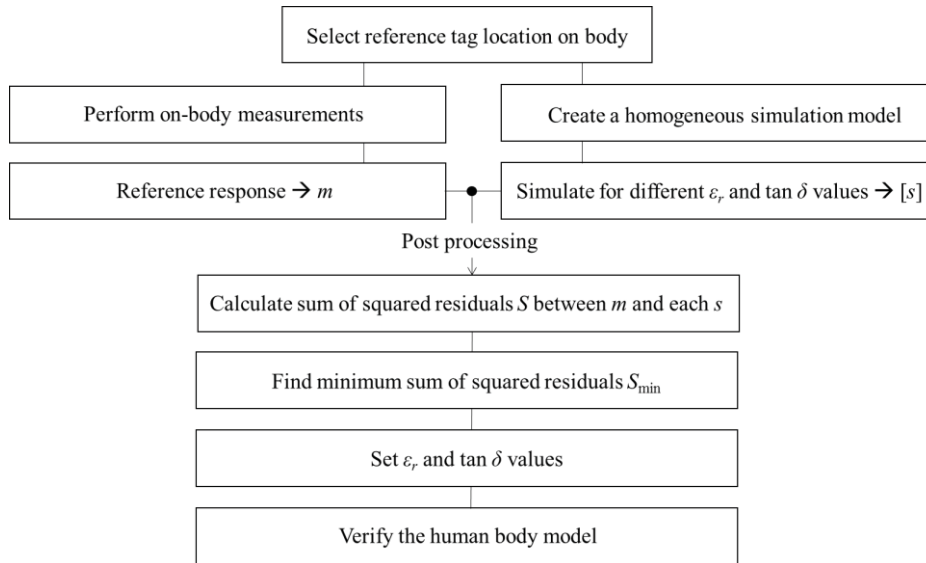


Figure 9. Flow chart for modeling the human body for UHF RFID body-centric systems for arbitrary tag location on body. The reference response  $m$  corresponds to any desired tag performance metric. The simulated solutions constitute a matrix  $[s]$  of the possible combinations of  $\epsilon_r$  and  $\tan \delta$  within specified boundaries.

Next, using an electromagnetic solver, a homogeneous dielectric human body model representing the tag location with fixed realistic dimensions is constructed. The model is assigned with the dielectric parameters  $\epsilon_r$  and  $\tan \delta$ . As the model dimensions are fixed, the parameters  $\epsilon_r$  and  $\tan \delta$  will account for the differences

in body shapes and tissue proportions between different individuals. The values of  $\epsilon_r$  and  $\tan \delta$  are selected so that the sum of squared residuals between the measured and simulated reference tag on-body responses is minimized. The measured reference tag response  $m(f_i, p_i)$  consists of  $n$  data pairs, where  $i = 1 \dots n$ , and  $n$  equals the number of frequency points over the considered frequency range. The pair  $(f_i, p_i)$  consists of the frequency variable  $f_i$  and the measured reference tag on-body performance metric  $p_i$ . For each combination  $\beta$  of  $\epsilon_r$  and  $\tan \delta$ , there exists a simulated reference tag performance solution  $s(f_i, p_i(\beta))$ . Using these notations, the sum of squared residuals is calculated as

$$S = \sum_{i=1}^n r_i^2, \quad (28)$$

where the residual  $r_i$  is defined as the difference between the measured and simulated tag on-body performance such that

$$r_i = p_i - p_i(\beta). \quad (29)$$

The values of  $\epsilon_r$  and  $\tan \delta$  are selected so that  $S$  is minimized. Finally, the human body model is verified for an arbitrary tag attached to the body location for which the model is developed.

In [II], the methodology presented in Fig. 9 was utilized to create a human body model for the three case studies in Fig. 8. The measured average read ranges in Fig. 8 were considered as the reference responses  $m(f_i, p_i)$ . For the arm and head cases, a cylinder was chosen to represent the tag location, whereas for the chest case, an elliptical model was chosen. Realistic dimensions were assigned to each model to mimic the body part. The considered frequency range was 860–960 MHz, and  $n$  was selected to 101. Using ANSYS HFSS, the read range of the dipole tag on Kapton platform (Fig. 7) was simulated according to (20) for  $\chi_{pol} = 1$  on each model. The simulated results are presented in [II]. The model parameters were swept for  $\epsilon_r = 5$ –50 with 0.5-step and for  $\tan \delta = 0.2$ –0.5 with 0.01-step, to cover the values measured from human tissues [73]. For each combination  $\beta$ , the sum of squared residuals  $S$  was calculated according to (28). The values of  $\epsilon_r$  and  $\tan \delta$  were chosen for which  $S = S_{\min}$ . The results are summarized in Table 5.

Table 5. An average statistical catalog of human body models for 860–960 MHz.

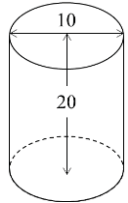
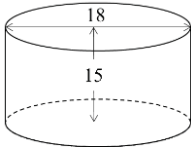
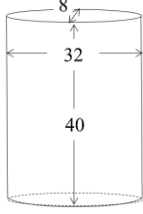
Application	UHF RFID human body model [cm]	Target group			
		Female		Male	
		$\epsilon_r$	$\tan \delta$	$\epsilon_r$	$\tan \delta$
Arm (Cylinder)		13.5	0.24	15.0	0.29
Head (Cylinder)		5.0	0.50	5.0	0.50
Chest (Ellipse)		33.0	0.17	33.0	0.17

Table 5 represents one possible statistical catalog of human body models. A wearable antenna designer would select the model dimensions according to the application (tag location) and set the model parameters according to the target group (subject). It is worth noticing that in future the catalog may be extended to cover all possible tag locations. Further, any desired division may be chosen for the target group. As the total time to complete one set of measurements for a given subject and tag location is rather short, the desired catalog may be derived time efficiently.

For the human body model verification purpose, two electro-textile dipole tags were used. The details of these tags are presented in [II]. Here it is sufficient to present the results for one of the electro-textile tags; the copper fabric tag implemented on cotton fabric ( $\epsilon_r = 1.8$  and  $\tan \delta = 0.018$ ) substrate. In simulations, the copper fabric was modeled as an infinitely thin conductor with a sheet resistance value of  $0.40 \Omega/\text{sq}$ . [v][III][IV]. The electro-textile tag on-body measurements were conducted and repeated similarly as for the dipole tag on Kapton platform. The verification results are given in Fig. 10.



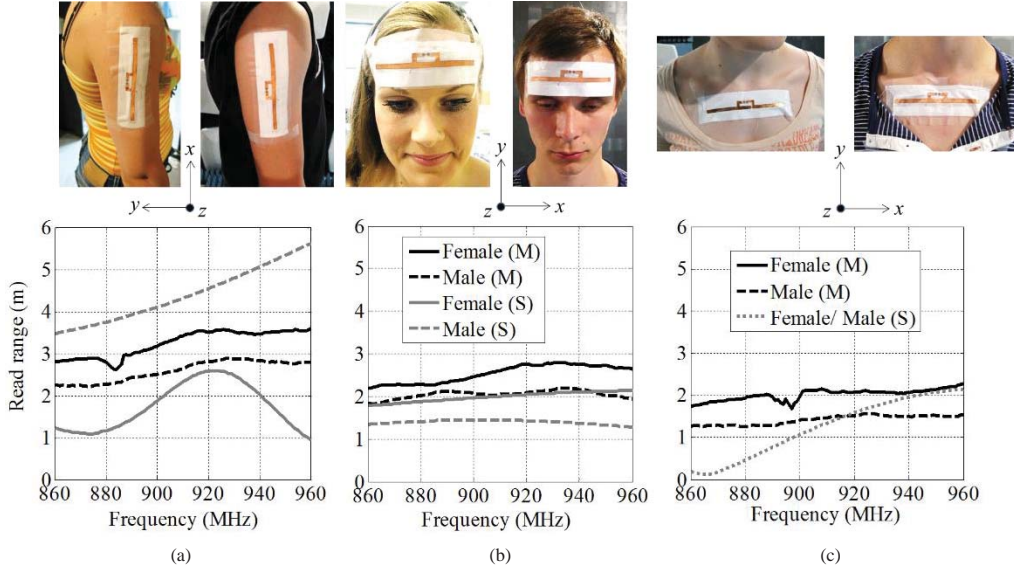


Figure 10. Electro-textile tag measured (M) on-body and simulated (S) on-model (Table 5) read ranges in  $+z$ -direction for female and male for; (a) upper arm, H-plane ( $yz$ -plane); (b) head, E-plane ( $xz$ -plane); and (c) chest, E-plane ( $xz$ -plane).

As expected, Fig. 10 shows that the electro-textile tag antenna on-body quality factor is low, indicating low tag antenna radiation efficiency. Of the three body models used, the head model is estimating the tag performance with highest accuracy. In terms of maximum deviation from measured on-body read range, the tolerance values for 860–960 MHz for the catalog in Table 4 are  $\pm 2.5$  meters. For a single case, the tolerance values are as low as  $\pm 0.8$  meters. It is important to note that the derived body model parameters  $\epsilon_r$  and  $\tan \delta$  are strongly correlated with the reference tag on-body location and attachment. Practically, it is challenging to attach the electro-textile tag perfectly similarly at identical locations as the reference tag. Particularly, when the tag is notably bent on the body surface, such as for the arm case, the body model uncertainty is increased. This is supported by Fig. 10. Thus, within the limits of expected uncertainties, it may be concluded that the body models have been successful. In summary, the modeling methodology of the human body can be quickly and easily adopted in practice to initiate the design of wearable antennas in body-centric systems.

### 3 WEARABLE ANTENNAS IN WIRELESS BODY-CENTRIC SYSTEMS

The wireless body-centric system is typically classified according to the nature of the used communication link (Fig. 11) [7]. Off-body communication takes place from off-body to an on-body device or system. On-body networks and wearable systems utilize on-body communication. Finally, in-body communication is established between medical implants and on-body sensor networks.

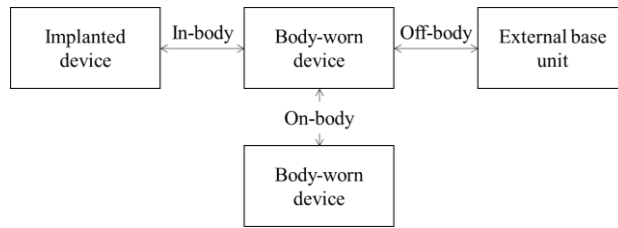


Figure 11. Classification of wireless body-centric channels.

Although the nature of the communication links differ significantly, the body-worn antenna is one of the key components in each of them. In many applications, an integrated system is using all three classes of communication. The wireless RFID-inspired brain-machine interface (BMI) system, envisaged Fig. 12, is such a system [I][vi]–[viii]. BMI systems have the enormous potential to provide a therapeutic technology for improving the life quality of people suffering from severely disabling neurological conditions, such as spinal cord injury and stroke. However, one of the main challenges towards clinically viable BMI systems is the lack of implantable electronics that last for several decades. This calls for miniature implantable devices embedding neural sensor electrodes, integrated electronics, and transmit antennas for power and data telemetry. From safety point of view, short range near-field RFID technology is an ultimate solution to realize wireless inductive powering of and communication with the implant [I]. The technology enables chronically implantable battery-free cortical implants composed of a loop antenna, an array of neural recording electrodes, and an ultra-low-power integrated circuit. The RFID principle is utilized as the in-body communication link between the battery-free cortical implant and the body-worn sensor network including the transmitting loop antenna. The neural data is sent over an off-body communication link to an external unit that decodes the data and controls artificial actuators.

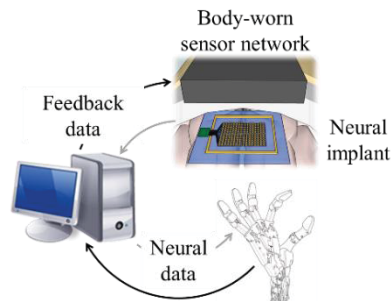


Figure 12. An RFID-inspired brain-machine interface system [I]. The picture of the robotic arm was taken from [74].

### 3.1 Wearable antenna design challenges

In general, a body-centric system is a highly interdisciplinary field of technology. The overall system quality relies on the performance of the system single components and entities, and their ability to communicate and interoperate efficiently and reliably with one another. This puts unique stringent requirements for the wearable antennas that encourage the RF community to explore novel design methodologies and advanced antenna materials.

One of the prime challenges in wearable antenna implementation is to achieve structures that enables seamless integration with clothing without compromising on the antenna performance. Copper is typically used as the conductive antenna element due to its superior conductivity. However, in wearable applications, the lack of structural flexibility prevents it from effectively conform to the surface. This calls for lightweight textile materials that provide competitive RF characteristics. Another issue is related to the durability of the wearable antenna materials [ix]. Integrated into clothing they are exposed to various environmental effects, including humidity and dirt, and they are vulnerable to bending and stretching deformations, as well as mechanical compression.

Although promising textile material candidates are available for wearable antennas, their fundamental high frequency characteristics and modeling parameters need to be established and verified before they can fully be adopted in the field of body-centric systems. This was the main objective in [III]–[V]. As chapter 4 presents, the outcome was innovative optimization methodologies for future novel wearable antennas that form an important contribution to the state of the art.

### 3.2 Electro-textiles for seamless and robust integration with clothing

Although electrically active textiles, or electro-textiles, with computational features have been of interest for over a decade [75][76], their use for electrical functions is a relatively new concept. The kernel of this concept is the development of the enabling technologies and fabrication techniques for the large-scale manufacture of flexible and conformal sensing systems that are expected to have unique applications for personal healthcare, military industry, as well as consumer electronics [4][9][10][12][17][34][70][77][78]. They provide lightweight and transparent sensing resources that are easily integrated or shaped into clothing. Electro-textiles are created either by using conductive sewing threads in a computer assisted embroidery machine [x][76][79], or by plating or interpolating a non-conductive fabric surface with an alloy of metals or with pure metal [68][76]. The conductive threads are created from strands of conductive and non-conductive fibers. Although single metallic fiber may be used as the conductive thread, its thin fragile structure is vulnerable to external tension, which prevents its use in embroidery machine. Therefore, the non-conductive fibers are typically included to protect the conductive fibers and to add mechanical robustness, but without impairing the electrical functionality. In [I]–[V], the utilized Shieldex [80] thread is created from two strands of strong non-conductive nylon yarn, each plated with silver (silver content 55 g/10 000 m). Previous experience [ii][v][ix][xiii] assure that the thread poses good mechanical robustness and competitively low conduction losses compared to the characteristics of other reported conductive threads [76].

The laboratory-scale fabrication principle of embroidered tag antennas is illustrated in Fig. 13. First, the antenna design footprint is imported as an image file to a computer-installed embroidery system software. The software enables control over the stitching pattern and density. The ready-made stitching pattern is transformed to an embroidery file, which is uploaded in a computer-aided embroidery machine. The machine

embroiders the stitching pattern automatically. In Fig. 13, the bobbin thread is conductive, whereas the upper thread is conventional non-conductive sewing thread. Often, however, both the bobbin and upper threads are chosen to be conductive.

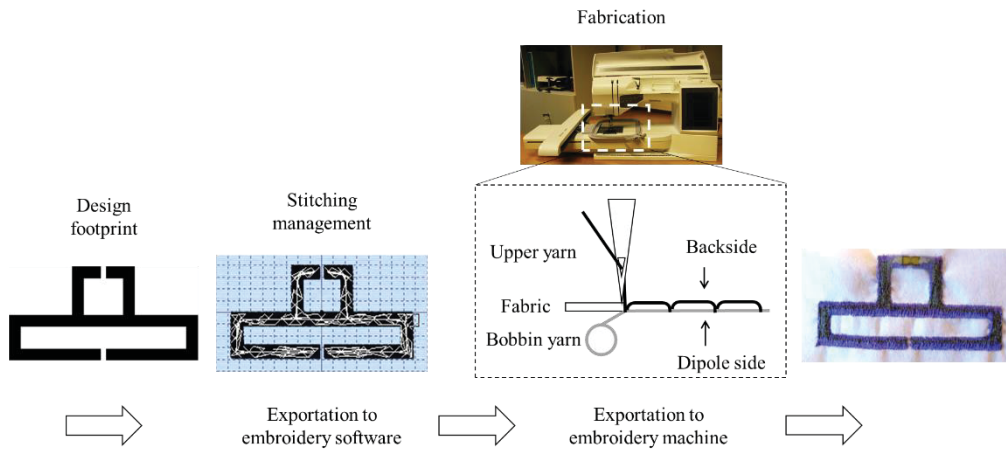


Figure 13. Laboratory-scale fabrication principle of embroidered tag antennas [x].

The tag antennas are typically embroidered onto thin regular polyester or cotton fabric [x][9][81]. In [I]–[V], the tag antennas were embroidered using Husqvarna Viking Designer Ruby embroidery machine onto 0.25-mm thick cotton fabric. The fabric relative permittivity and loss tangent were measured to 1.8 and 0.018, respectively, using the resonance method [82]. As the fabric is very thin and its losses are very small relative to the losses of conductive sewing thread, the presence of the cotton fabric will not affect the tag antenna performance.

Figure 14 shows four different conductive fabrics from Less EMF [83] that were studied in [III].

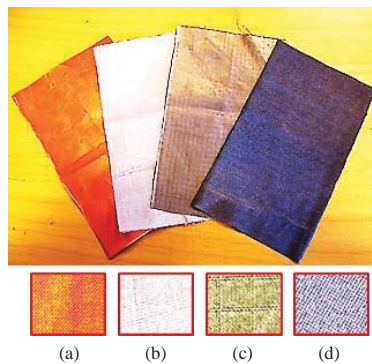


Figure 14. Conductive fabrics from LessEMF; (a) copper; (b) argenmesh; (c) ripstop; and (d) stretch.

The copper fabric is a pure copper plated smooth polyester fabric. The copper content is approximately 35%. Both the argenmesh and ripstop fabrics are nylon based and they use pure silver as conductor. The argenmesh fabric is interpolated with silver threads (silver content 55%), whereas the ripstop fabric has a

silver plating. Finally, the stretch fabric is a silver plated 76% nylon–24% elastic fiber fabric. The electrical properties of commercially available conductive fabrics vary greatly depending on the fabric type and how the surface is metal treated [IV]

### 3.3 Embroidered antenna durability

The metallized sewing threads are vulnerable to washing procedures as the metal particles are easily dissolved in water. Consequently, when the tag antenna is exposed to water its radiation efficiency is decreased. Already at low washing temperatures and low rotation speeds, this may appear as several meters free-space read range drop after few washing cycles [ix][84]. This is evidenced in Fig. 15, showing the read range degradation for an embroidered tag after three washing cycles with detergent in 40°C and 400 rpm. According to measurements, the tag antenna directivity was not affected by the washing operations [ix].

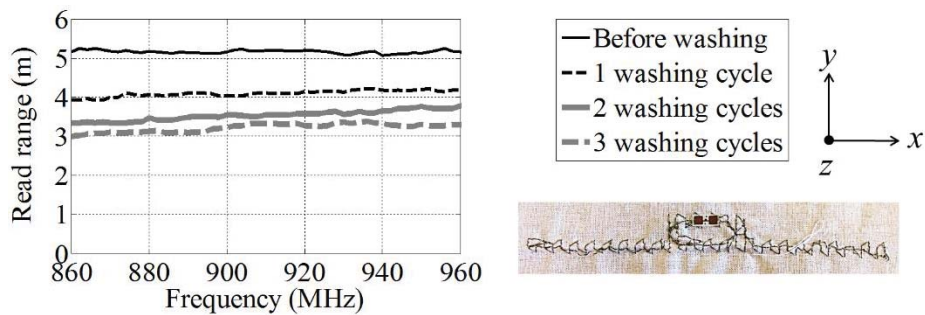


Figure 15. Measured free-space read range according to (20) in +z-direction for an embroidered tag washed three times. The NXP RFID IC is detached prior to each washing time. [ix]

Depending on the harshness of the used washing program, it was estimated that 7 to 23 washing cycles were required to reduce the tag antenna radiation efficiency to a level corresponding to 0.5 meter free-space read range [84]. Hence, a protection technique to reinforce the embroidered tag durability is a must before the wearable antennas may meet public acceptance. Such reinforcement is required to be hydrophobic and to maintain the flexibility of the tag antenna without impairing the tag performance. Polydimethylsiloxane (PDMS), a silicon based organic polymer, is a potential candidate that fulfills these requirements [ix][64][79][85]. It is a soft, hydrophobic, heat resistant, low loss, and flexible material. Figure 16 presents a PDMS immersed embroidered tag and its measured performance before and after immersion in PDMS, and after one washing cycle. The PDMS offers a powerful solution for the protection of both the tag antenna conductor and the RFID IC.

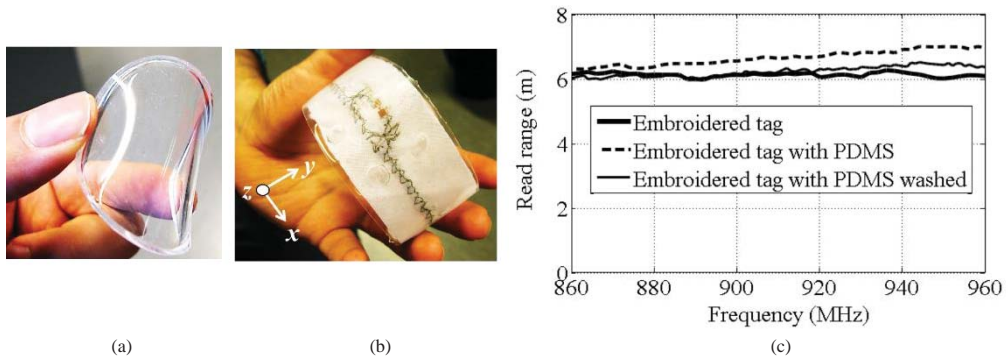


Figure 16. Reinforcement of embroidered tag durability; (a) pure PDMS [85]; (b) PDMS immersed embroidered tag with NXP RFID IC [ix]; (c) Measured embroidered tag free-space read range according to (20) in  $+z$ -direction [ix].

The PDMS polymer allows to be mixed with barium titanate, a high dielectric ferroelectric powder, to achieve a ceramic composite with desired permittivity [85], but without compromising on the flexibility and durability. Embedding embroidered tags into such high-permittivity material enables durable entities with built-in immunity to the human body.

## 4 FUNDAMENTAL CHARACTERISTICS OF ELECTRO-TEXTILES FOR WEARABLE UHF ANTENNAS

The electrical characterization of the electro-textiles in the microwave frequencies has been actively studied [76][79][86]. Particularly, the transmission line method is commonly used in which the S-parameters for a 50- $\Omega$  transmission line of the electro-textile is measured [79][86]. A common understanding is that higher conductive thread density in the electro-textile results in higher effective conductivity and consequently higher antenna radiation efficiency [76][79][87]. Also, a common practice is to align the conductive threads along the current flow in the antenna to keep the conduction losses as low as possible [81][87]. These phenomena seem to be very true when considering traditional characterization methods, in which the electro-textile structure to be characterized is assumed to be non-radiative. However, when the electro-textile forms the radiating antenna, the desired antenna performance is not guaranteed.

Majority of the proposed embroidered antennas are fabricated using high stitching densities and their measured performances are evaluated by comparing them with that of simulated or measured copper antenna [76][79][87]. Less attention is hence paid to the design and optimization of the thread distribution in the embroidered antenna pattern. Nevertheless, some steps towards modeling the embroidered electro-textiles have been taken. One approach is to model the embroidered antenna pattern as a uniform *conductor* layer with a given thickness and an effective conductivity [88]. The thickness is a function of stitching density and measured as the upper face of the embroidered pattern. The effective conductivity accounts for the overall antenna losses. Although a promising modeling technique is demonstrated, it faces some evident uncertainties that prevents it from properly account for all the electromagnetic effects related to the conductive threads forming the embroidered pattern of different stitching densities and distributions. The embroidered pattern thickness is not unambiguously defined; as the stitching density decreases, the pattern become highly irregular. Another issue is that the embroidered antenna uniform conductor model is not capable of predicting a possible change in the antenna electrical length when different stitching densities and patterns are used [ii][ix][81][87][88].

The uncertainty related to the embroidered antenna thickness may be eliminated by using the sheet resistance  $R_s$  for modeling the electro-textile [III][v]. This parameter is independent of the material thickness and may be extracted by combining reflectometry measurements and corresponding simulations [v]. The technique relies on the wireless measurement of the radar cross section (RCS) of a resonant scatterer fabricated of the electro-textile to be characterized. Its magnitude is strongly correlated with the scatterer conductive losses so that a relationship between the sheet resistance and RCS may be established. The searched  $R_s$  value for different electro-textiles is attained by comparing the magnitude of the measured RCS resonance with simulated RCS. The scatterer is modeled as a uniform infinitely thin conductor having the  $R_s$  as the only material parameter. Simulating the scatterer RCS with plane wave excitation for different  $R_s$  values, a correlation between measured peak magnitude RCS and  $R_s$  is found. The scatterer resonant mode is observed at a specific frequency, which is determined by the physical size of the scatterer.

In [III] this characterization method was utilized for the conductive fabrics presented in Fig. 14 and for two embroidered patterns. One of the embroidered patterns used thread along the current flow in the scatterer (contour), whereas the other used thread against the current flow (zigzag). The fabricated embroidered scatterers are shown in Fig. 17. The conductive fabric scatterers were implemented on 100  $\mu\text{m}$ -thick Kapton HN polyimide film ( $\epsilon_r = 3.5$  and  $\tan \delta = 0.0026$ ).

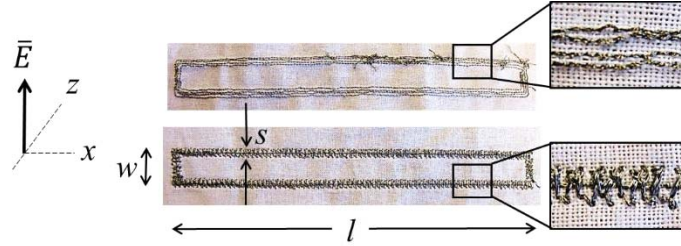


Figure 17. Contour (top) and zigzag (bottom) scatterers for wireless reflectometry measurements. The scatterers were embroidered using Shieldex conductive thread on 0.25-mm thick cotton fabric ( $\epsilon_r = 1.8$  and  $\tan \delta = 0.018$ ). The dimensions ( $l = 158$  mm,  $w = 16$  mm, and  $s = 3$  mm) correspond to the dimensions of a bulk copper scatterer on 100- $\mu\text{m}$  thick Kapton substrate resonating at 900 MHz. [III][v]

Using the measurement set-up and procedure in [v], a correlation between measured peak magnitude RCS and  $R_S$  was established as shown in Fig. 18. Using the results, sheet resistance values of 0.40  $\Omega/\text{sq}$ . for the copper fabric, 0.55  $\Omega/\text{sq}$ . for the ripstop fabric, 1.25  $\Omega/\text{sq}$ . for the stretch fabric and contour embroidery, 2.25  $\Omega/\text{sq}$ . for the argenmesh fabric, and 4.5  $\Omega/\text{sq}$ . for the zigzag embroidery were extracted [III].

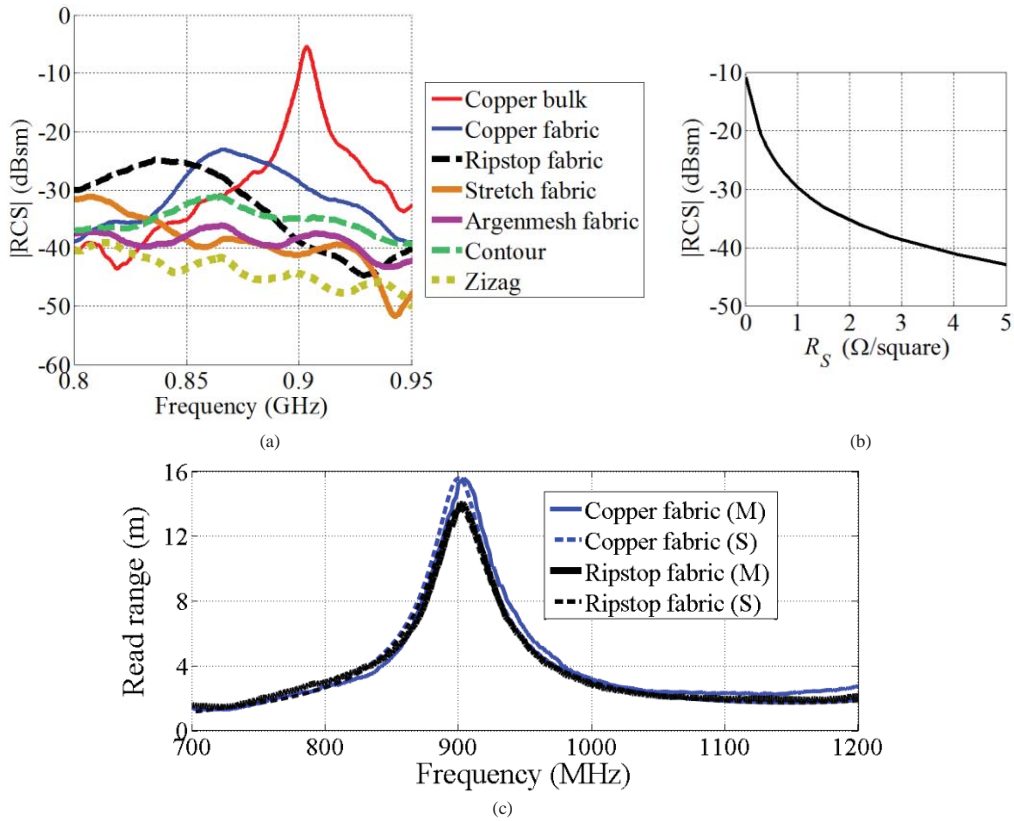


Figure 18. Sheet resistance  $R_S$  extraction for various electro-textiles using wireless reflectometry; (a) measurement results for the fabricated scatterers of various electro-textiles in horizontal (+y-direction) polarization for plane wave excitation; (b) correlation between measured peak RCS and  $R_S$ ; (c) measurement and simulation results in +z-direction for the reference patch tag in Fig. 5 when its ground plane is replaced by the copper and ripstop fabrics. [III][v]



The sheet resistance accuracy is related to the measured RCS. The correlation graph shows that small sheet resistance values are more accurate as a large RCS change will give a small sheet resistance change. This is reasonable. A low  $R_s$  value is linked with a narrow scatterer bandwidth and hence, with better selectivity. Consequently, the characterization method is only suitable for electro-textiles having sheet resistance values below approximately  $0.6 \Omega/\text{sq}$ . Further, the characterization method lacks to account for a possible change in the scatterer electrical length as only the magnitude of the measured RCS is considered and the electro-textile is assumed to behave as a conductor. This limits the method to be applied for electro-textiles that result in the same electrical length as bulk copper and whose conduction losses (ohmic losses) are small enough. The copper and ripstop fabrics fulfill these requirements [III][IV]. In [III], the ground plane of the reference patch tag antenna in Fig. 5 was replaced by the copper and ripstop fabrics. In ANSYS HFSS this corresponded to the replacement of the ground plane by an infinitely thin sheet having sheet resistance values of  $0.40 \Omega/\text{sq}$  and  $0.55 \Omega/\text{sq}$  for the copper and ripstop fabrics, respectively. The measured (22) and simulated (20) free-space read ranges for the reference patch tag with electro-textile ground planes are presented in Fig. 18. Indeed, the characterization method is well-suited for these highly conductive fabrics.

The main motivation in [IV] and [V] was to establish applicable methodologies for the characterization and optimization of an arbitrary electro-textile for the development of wearable UHF RFID patch tag antennas. The steps that were taken to fulfill these objectives are considered through the following case studies. As a fundamental starting point, *all* electro-textiles were considered to hold *dissipative dielectric* characteristics to properly account for the conduction losses and a possible change in the antenna electrical length. From modeling point of view, this corresponded to the introduction of a *complex sheet impedance*  $Z_s$  parameter. Depending on the electro-textile stitching pattern and density, and on the implementation of the metallization, the sheet impedance is either purely real or complex. For an arbitrary and fixed electro-textile, the sheet impedance may be extracted using the methodology presented in Fig. 19. The performance metrics are selected to be appropriate for the wearable antenna application. The agreement between measured and simulated antenna performance metrics is considered acceptable if it is within the interval of expected uncertainties related to the antenna fabrication technique and measurements [II].

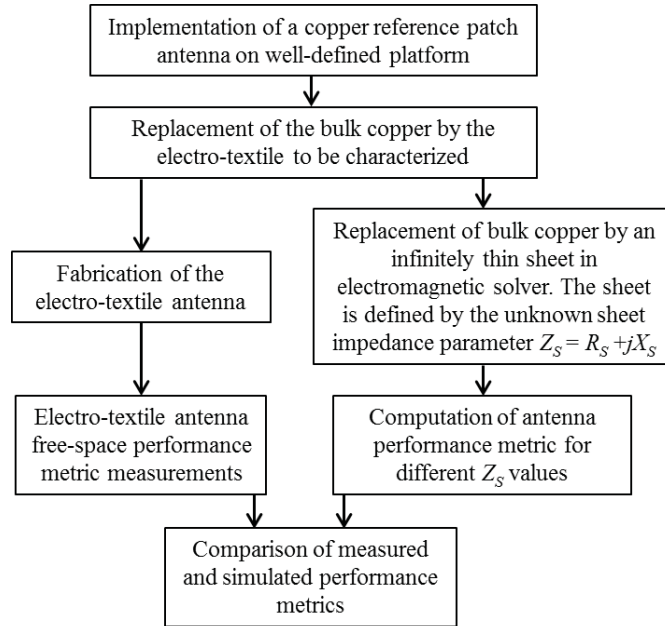


Figure 19. Applicable methodology for the characterization of an arbitrary and fixed antenna electro-textile.

#### 4.1 Case study 1: Electro-textiles for which $Z_s$ is real

Some conductive fabrics do not change the antenna electrical length or cause any impedance detuning compared to bulk copper. They primarily affect the tag performance by introducing additional ohmic losses  $R_{ohmic}$ , which is seen as a decrease in the antenna gain. For such conductive fabrics, the sheet impedance imaginary part approaches zero, and consequently, they can be approximated as conductors whose sheet resistance  $R_s$  is larger than that of bulk copper. This is the case for the copper, ripstop, and argenmesh fabrics in Fig. 14 [III][IV]. The sheet resistance values for the copper and ripstop fabrics were extracted from Fig. 18. For the argenmesh fabric, the procedure in Fig. 19 was used for the case when the reference patch tag (Fig. 5) ground plane was replaced by the argenmesh fabric. Figure 20 shows that the argenmesh fabric sheet resistance value is  $0.65 \Omega/\text{sq}$ .

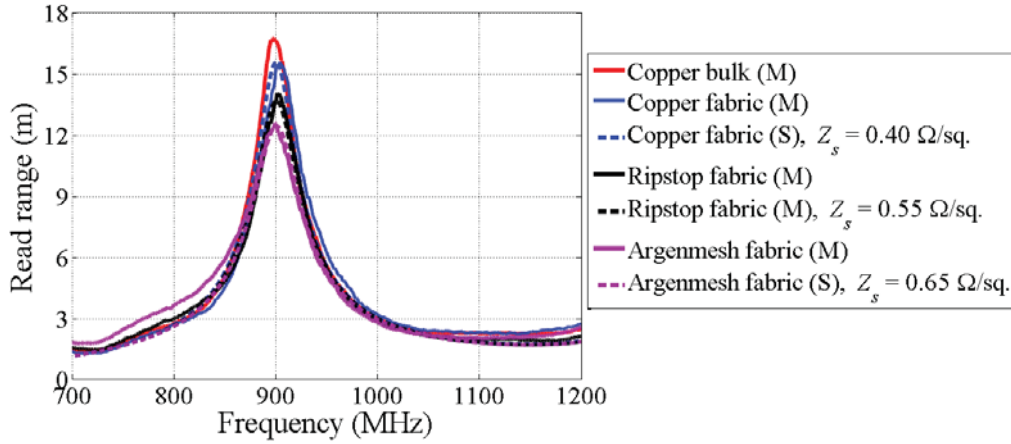


Figure 20. Measured (M) and simulated (S) free-space read ranges according to (22) and (20), respectively, in  $+z$ -direction for the reference patch tag with conductive fabric ground plane. The considered electro-textiles may be approximated as pure conductors.

Electro-textiles having a purely real sheet impedance value do not change the tag antenna directivity [III][IV].

#### 4.2 Case study 2: Electro-textiles for which $Z_s$ is complex

All embroidered electro-textiles have a complex sheet impedance value. The sheet impedance is also complex for some conductive fabrics. In [III] and [IV] this statement was systematically verified by separately replacing the reference patch tag ground plane and top patch with various electro-textiles. The fabricated embroidered electro-textile prototypes are presented in Fig. 21.

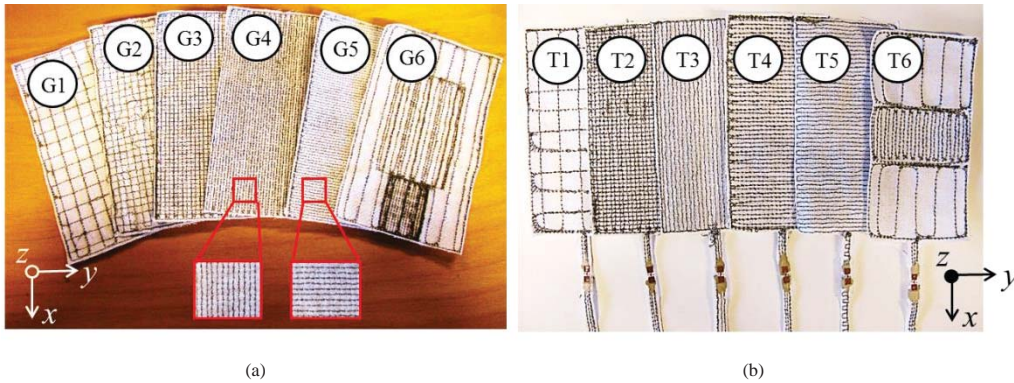
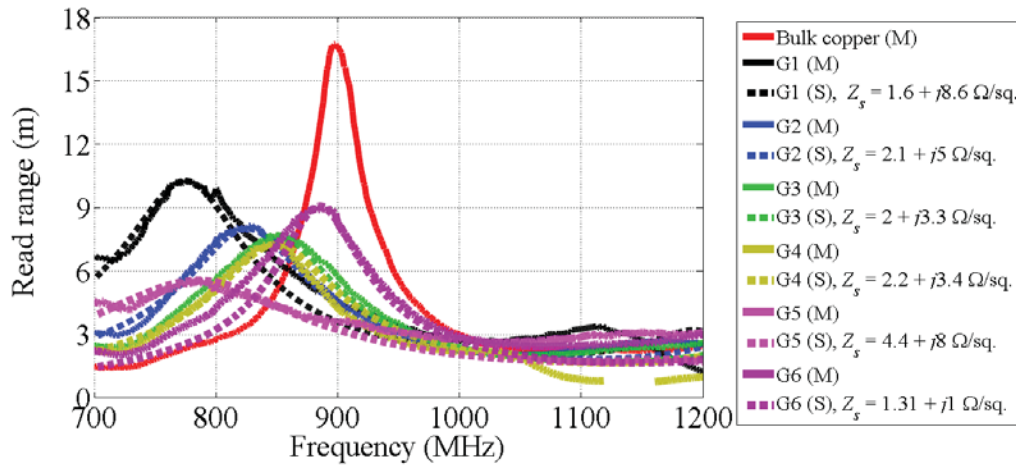
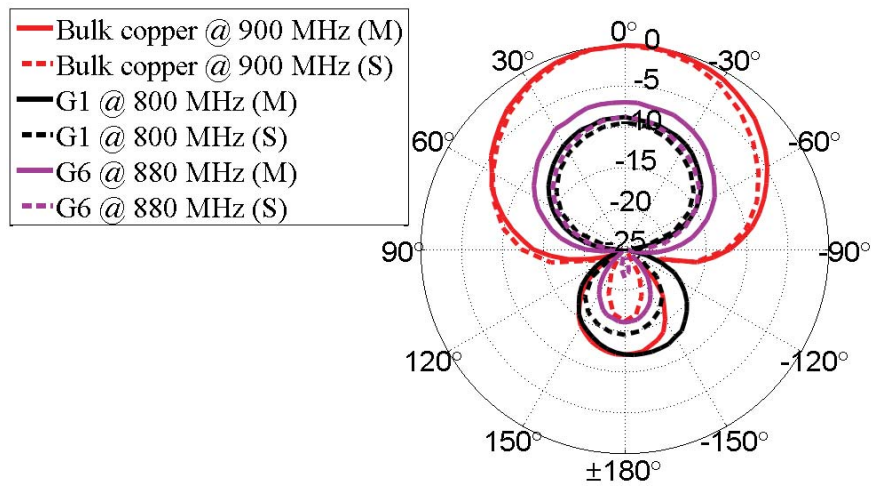


Figure 21. Embroidered prototypes; (a) ground planes: (G1) embroidery 1, square density  $3\lambda/100$ ; (G2) embroidery 2, square density  $3\lambda/200$ ; (G3) embroidery 3, square density  $9\lambda/1000$ ; (G4) embroidery 4, vertical line density  $3\lambda/500$ ; (G5) embroidery 5, horizontal line density  $3\lambda/500$ ; and (G6) embroidery 6, vertical line densities  $3\lambda/100$ ,  $9\lambda/1000$ , and  $3\lambda/500$ ; (b) top patches: (T1) embroidery 1, square density  $3\lambda/100$ ; (T2) embroidery 2, square density  $3\lambda/500$ ; (T3) embroidery 3, vertical line density  $3\lambda/500$ ; (T4) embroidery 4, horizontal line density  $3\lambda/500$ ; (T5) embroidery 5, horizontal line density  $3\lambda/500$ ; and (T6) embroidery 6, vertical line densities  $3\lambda/100$  and  $3\lambda/500$ . Vertical line density of  $3\lambda/500$  was used for the feed in embroideries 1–4 and 6, whereas horizontal line density of  $3\lambda/500$  was used for the feed in embroidery 5. The wavelength corresponds to 900 MHz. The square density corresponds to the square side length, whereas the line density corresponds to the distance between two lines.

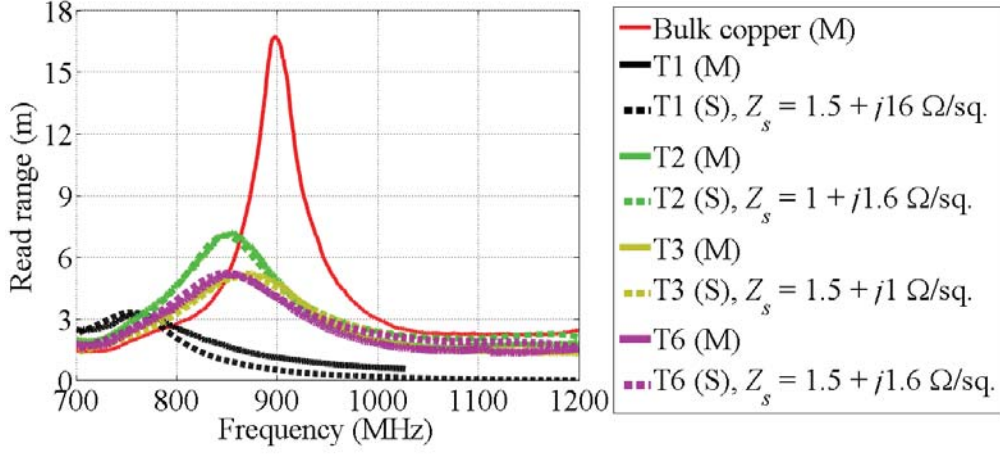
The prototypes were characterized in free-space using the procedure given in Fig. 19. The tag read range and the tag antenna normalized E-plane ( $xz$ -plane,  $\phi = 0^\circ$ ) power pattern were chosen as the performance metrics. Since the reference patch tag ground plane remained as solid copper for the top patch cases, low tag antenna back lobe level was measured for all top patch prototypes. The most valuable characterization results are given in Fig. 22.



(a)



(b)



(c)

Figure 22. Embroidered prototype characterization; (a) Measured (M) and simulated (S) free-space read ranges according to (22) and (20), respectively, in  $+z$ -direction for the reference patch tag with embroidered ground plane; (b) Free-space E-plane power patterns normalized to the bulk copper (reference) patch tag threshold power  $P_{th, \min}(\theta, \phi)$  according to (25); (c) Measured (M) and simulated (S) reference patch tag free-space read range in  $+z$ -direction with embroidered top patch. Prototypes T4 and T5 did not yield any measurable antenna response due to significant cross-polarization level.

In general, embroidered patterns forcing the current to take a long path result in severe tag antenna input impedance detuning towards lower frequencies with respect to the reference patch tag antenna. For ground plane patterns, also a notable change in the tag antenna directivity is observed. This strongly suggests that the embroidered pattern increases the tag antenna input inductance. Equivalently, the embroidered pattern electrical length is longer compared to that of a copper conductor. When the embroidered pattern shape and size is fixed, the sheet reactance is directly proportional to the stitching density. This is evidenced for the squared stitching patterns in Fig. 23.

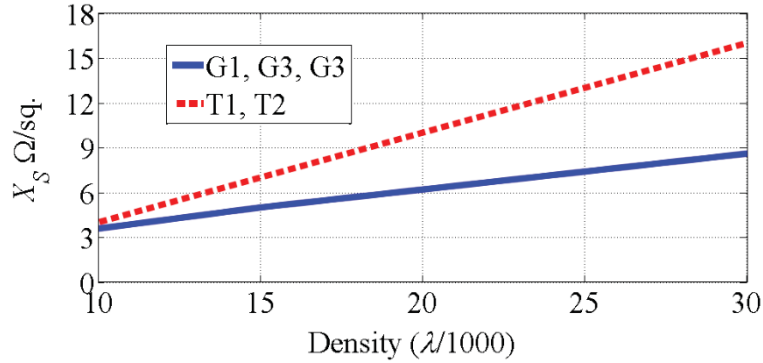


Figure 23. Correlation between square-shaped embroidery sheet impedance imaginary part and stitching density. The wavelength corresponds to 900 MHz. A small density corresponds to small squares.

As expected, deploying the threads against the reference tag antenna current flow results in heavy cross-polarization losses. For the top patches T4 and T5, the losses are high enough to prevent the tag IC from receiving enough power to power up. Based on simulations, the tag antenna gain in  $+z$ -direction is decreased

with decreased square density for the ground planes G1–G3. For the top patches T1 and T2, the reverse effect was simulated. Obviously, the conduction losses are not only correlated with the stitching density and the amount of overlapping of threads [III][IV][88], but also on the thread distribution within the embroidered pattern with respect to the surface current distribution in a corresponding bulk conductor.

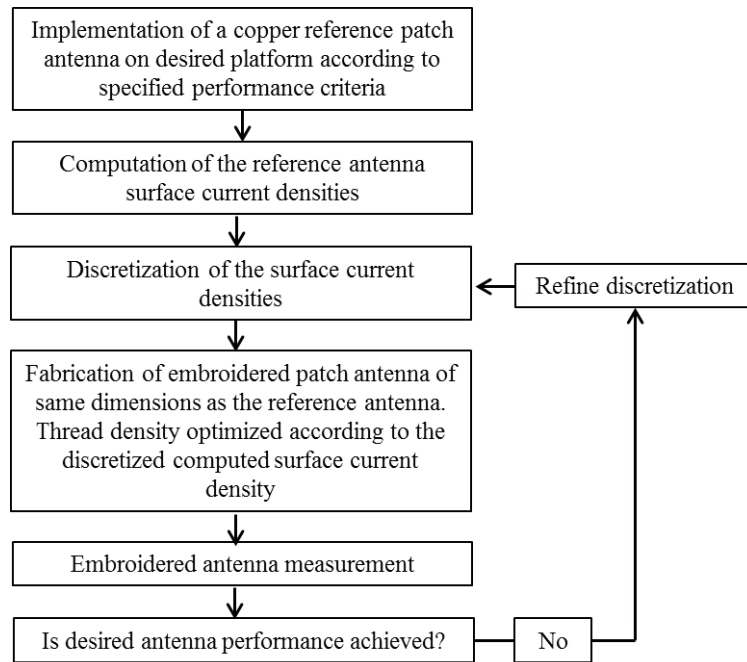


Figure 24. Applicable methodology for the optimization of embroidered antenna patterns.

Based on the observations, a methodology shown in Fig. 24 for the optimization of embroidered antenna patterns was developed. Using this methodology, the prototypes G6 and T6 were implemented. The discretized surface current densities in the reference patch tag antenna ground plane and top patch (Fig. 25) were used for the optimization of the stitching patterns and densities. Regions with high surface current densities were converted to high stitching densities to minimize the tag antenna input impedance detuning effect. Regions with low surface current densities were converted to low stitching densities to minimize the overall antenna conduction losses. Threads were deployed along the reference patch tag antenna current flow to prevent polarization losses.

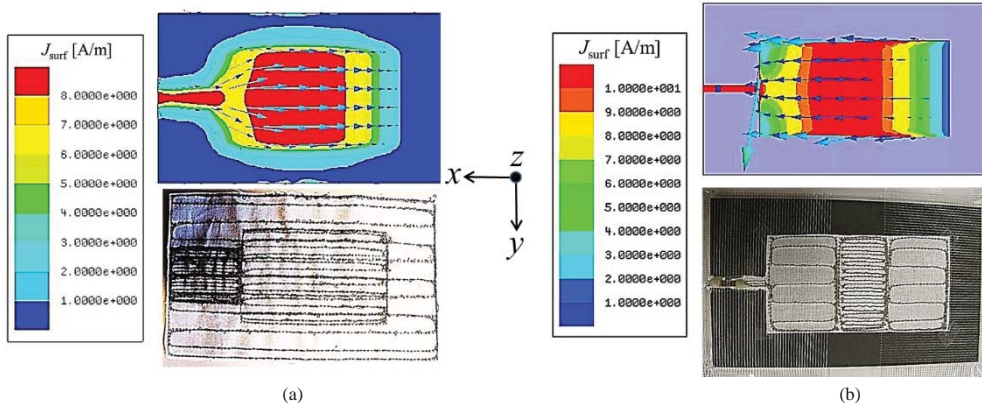


Figure 25. Free-space simulated surface current density at 900 MHz in the reference patch tag antenna (a) ground plane and (b) top patch. The antenna accepts 40 mW of power. The antenna has vertical linear polarization.

The G6 structure achieves low sheet resistance and reactance values and consequently, the antenna poses operational frequency close to 900 MHz, small back lobe level, and maximized read range (Fig. 22). Ideally, the sheet reactance becomes zero valued, and the embroidered pattern approximates conductor characteristics. Practically, however, the embroidered pattern electrical length is always longer compared to that in a conductor and thus, the sheet reactance value never reaches zero. The top patch surface current density was refined and prototype T7 with increased thread density along the top patch length ( $x$ -direction) was fabricated. As Fig. 26 presents, this single iteration step gained one meter more read range. This is an extremely important result for the promotion of industrial garment-integrated wearable antennas.

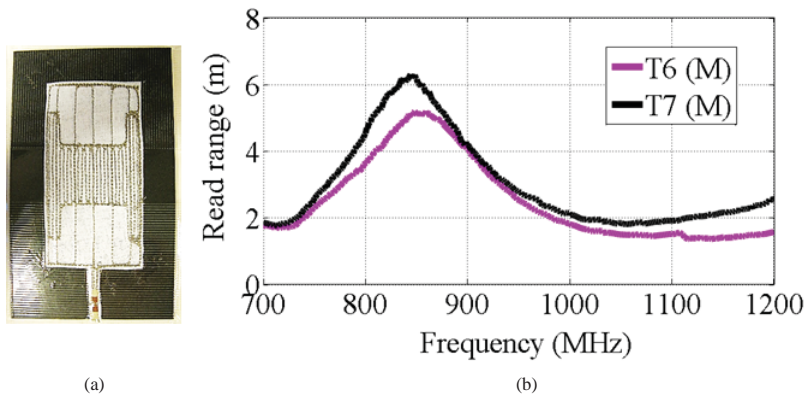
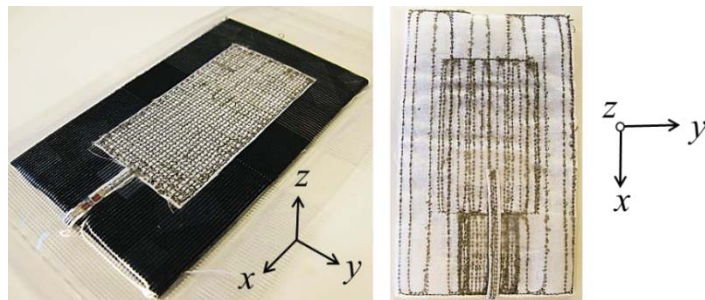


Figure 26. (a) Top patch embroidery T7; (b) Measured free-space read ranges according to (22) in  $+z$ -direction for the reference patch tag with top patch embroideries T6 and T7. A single iteration realized in T7 prototype gained improved tag performance.

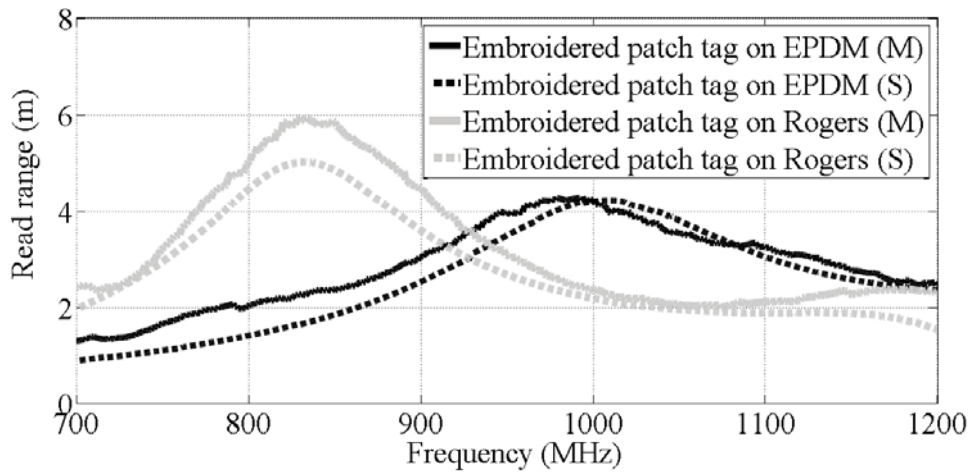
The characterization methodology in Fig. 19 was used to verify that the sheet impedance is complex for the stretch fabric in Fig. 14 [IV].

### 4.3 Case study 3: Electro-textile UHF RFID patch tags for wearable applications

A fully wearable embroidered patch tag was fabricated by utilizing the characterized embroideries G6 and T2. The Rogers RT/Duroid 5880 substrate was replaced by 3-mm thick flexible EPDM (Ethylene-Propylene-Diene-Monomer) foam [89] with the dielectric properties  $\epsilon_r = 1.23$  and  $\tan \delta = 0.02$ . The EPDM foam dimensions were the same as for the Rogers substrate. The electro-textiles were attached to the foam substrate by enclosing the tag in a vacuum pack. This way no additional mounting materials were required and the tag characterization accuracy was improved. The tag enclosure in vacuum pack compressed the foam substrate thickness to 2.7 mm. The embroidered patch tag free-space performance is presented in Fig. 27. The change from the low-loss Rogers substrate to the low-permittivity EPDM foam substrate degrades the read range and shifts the tag resonance frequency to 990 MHz. The influence of the EPDM foam substrate on the embroidered patch tag performance is highlighted by incorporating the read range result for the embroideries G6 and T2 when placed on Rogers substrate. A maximum disagreement of 5 dB is observed between the measured and simulated power patterns in Fig. 27. A similar disagreement is found in Figs. 5 and 22. The disagreement is explained by the limited measurement accuracies of the threshold power levels in (25) [III].

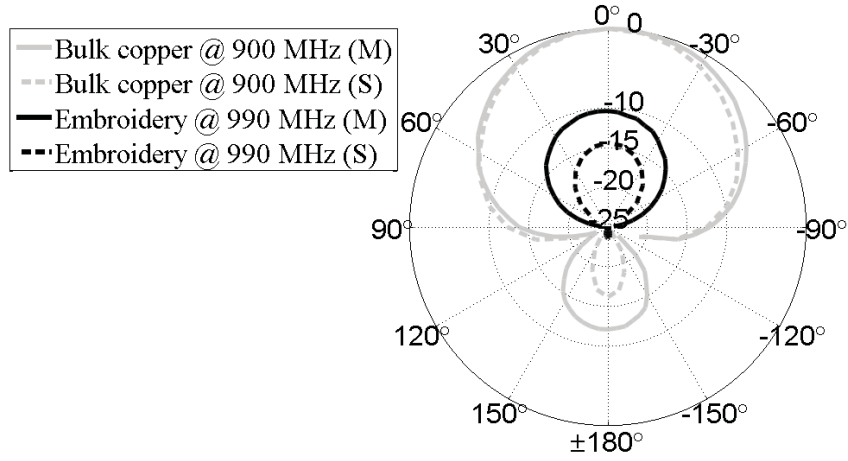


(a)



(b)





(c)  
 Figure 27. (a) Embroidered top patch T2 and ground plane G6 placed over EPDM foam substrate; (b) Measured (M) and simulated (S) free-space read ranges according to (22) and (20), respectively, in  $+z$ -direction for the embroidered patch tag on EPDM foam and on Rogers substrates; (c) Free-space E-plane ( $xz$ -plane,  $\phi = 0^\circ$ ) power patterns normalized to the bulk copper (reference) patch tag threshold power  $P_{th,min}(\theta, \phi)$  according to (25).

The results validate the hypothesis that a complex sheet impedance is required to properly account for the electromagnetic effects related to the embroidered patterns. The embroidered patch tag antenna achieves extremely low back lobe level, which denotes robust platform tolerance. The 4-meter peak read range sets a benchmark for future embroidered patch antenna designs.

For comparison purpose, a copper fabric patch tag on EPDM foam substrate was designed and fabricated [V]. For fair comparison, the dimensions of the copper fabric tag was fixed to correspond to the size of the embroidered one. Simulations were conducted using ANSYS HFSS. The copper fabric was modeled with the sheet resistance values  $0.15 \Omega/\text{sq.}$  and  $0.40 \Omega/\text{sq.}$  for the top patch and ground plane, respectively [IV]. The difference in the copper fabric sheet resistance values is descended from the inaccuracies related to the electro-textile antenna fabrication technique, which is used in the characterization methodology presented in Fig. 19. These inaccuracies are higher for the copper fabric top patch compared to the copper fabric ground plane. The tag antenna was tuned to achieve conjugate matching with the NXP RFID IC input impedance at 866 MHz by introducing slots in the tag antenna top patch (Fig. 28). The parameters  $h$ ,  $s$ , and  $d$  were adjusted to attain desired operational frequency. The copper fabric patch tag free-space read range is presented in Fig. 28. The measured tag antenna back lobe level was low. The copper fabric conductor model predicts the copper fabric patch tag performance accurately.

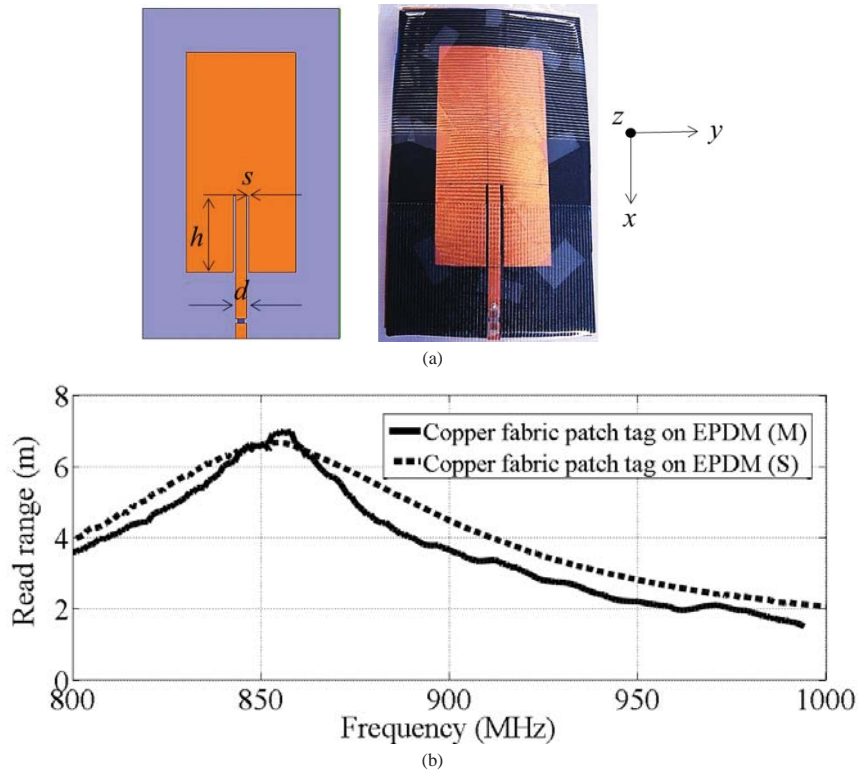


Figure 28. (a) Copper fabric patch tag on EPDM foam substrate enclosed in vacuum pack. The thickness of the tag was measured to 4.5 mm. The tuning parameters are  $s = 1$  mm,  $h = 35$  mm, and  $d = 4$  mm; (b) Measured (M) and simulated (S) free-space read ranges according to (22) and (20), respectively, in  $+z$ -direction for the copper fabric patch tag on EPDM foam substrate.

To verify the tag platform tolerance, the on-body H-plane ( $yz$ -plane) read ranges for the embroidered and copper fabric patch tags were measured in office environment [V]. The measurement set-up is shown in Fig. 29. The read ranges were measured along the measurement line, towards which the linearly polarized reader antenna has its main beam. The electro-textile tags were attached to the arm at the same height as the reader antenna. The tags were separated from the arm with a 0.7-mm thin shirt. A thin shirt was chosen for the evaluation of a worst case scenario. The reader antenna to tag distance  $d$  was chosen short enough to minimize reflections from the environment but long enough to assure far-field measurements. The measured electro-textile patch tag read ranges in air and on-body are given in Fig. 29.

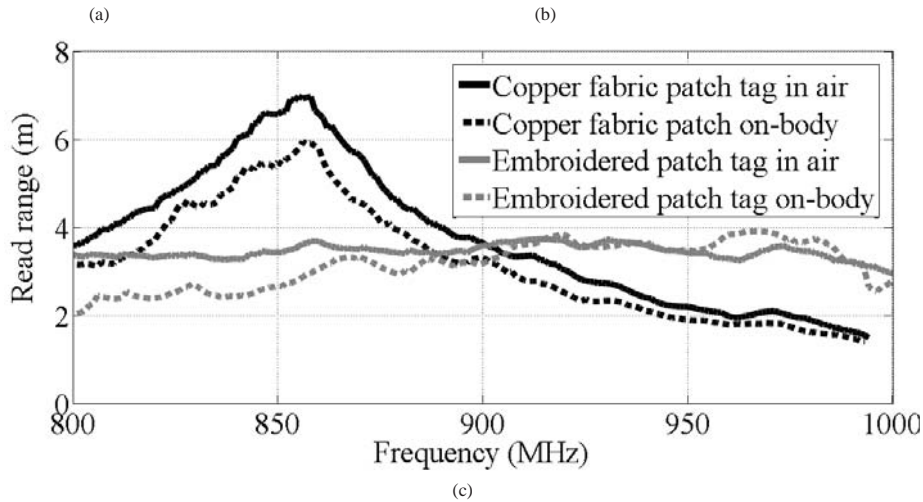
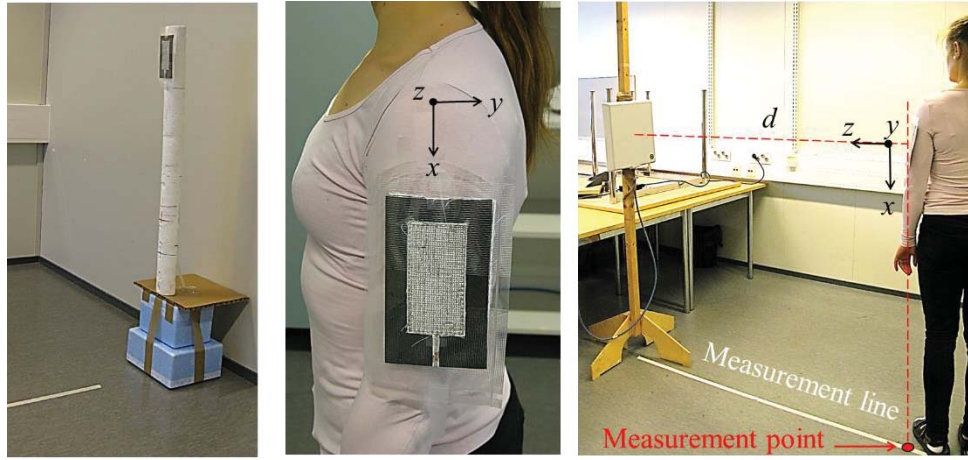


Figure 29. Measurement set-up in office environment in (a) air and (b) on-body. The same measurement set-up was used for the copper fabric patch tag; (c) Measured read ranges according to (22) in  $+z$ -direction for the electro-textile patch tags on EPDM foam substrate in office environment in air and on-body.

In terms of platform tolerance, the embroidered patch tag features inherently excellent antenna to body isolation. This highlights the importance of the proposed methodology for the optimization of embroidered antenna patterns presented in Fig. 24. As observed from previous sections, the T2 and G6 prototypes provided tag read ranges of 5 and 9 meters, respectively, on low-loss antenna substrate. A nearly 4-meter on-body read range for the fully embroidered patch tag on EPDM foam substrate is hence considered as a milestone of paramount importance in the development towards wearable intelligence.

The feasibility of the electro-textile patch tags was elaborated further by performing indoor Received Signal Strength (RSS) measurements [V]. Power measurements, such as RSS, applied for indoor localization [90]. Typically, Wireless Local Area Networks (WLAN) signals are employed for such purposes [91]. Nevertheless, any wireless signal available in indoor scenarios may be exploited. RFID-inspired localization systems [92] enable portable solutions in the form of wearable RFID tags. Such systems are highly demanded for health

state monitoring, object tracking, and security. Particularly, passive UHF RFID provides an attractive technology for indoor localization thanks to its contactless communication, none-line of sight readability, and low-cost features. Similarly with WLAN RSS approaches, the measured backscattered power at the receiver from the passive RFID tags convey information needed for localization. Garment-integrated wearable antennas constitute a key component of an indoor RFID system for human localization and positioning. The wearable antenna design and material choices are directly affecting the achieved localization accuracy. This was the prime motivation behind the elaboration on the feasibility of the wearable patch tags in the context of indoor RSS measurements [V].

The RSS measurements were carried out in the indoor office environment shown in Fig. 29. Additional measurement lines were defined to cover an observation area of half a hemisphere as pointed out in Fig. 30. The main beam of the reader antenna was towards line 6. The reader antenna gain is 9.5 dBi. The transmitter transmission frequency was chosen to 866 MHz. In order to not exceed the maximum power allowed to be transmitted from the output port with the used measurement set-up without exceeding the regulated isotropically radiated power of 3.28 W, the transmitter output port power was set to 26.9 dBm.

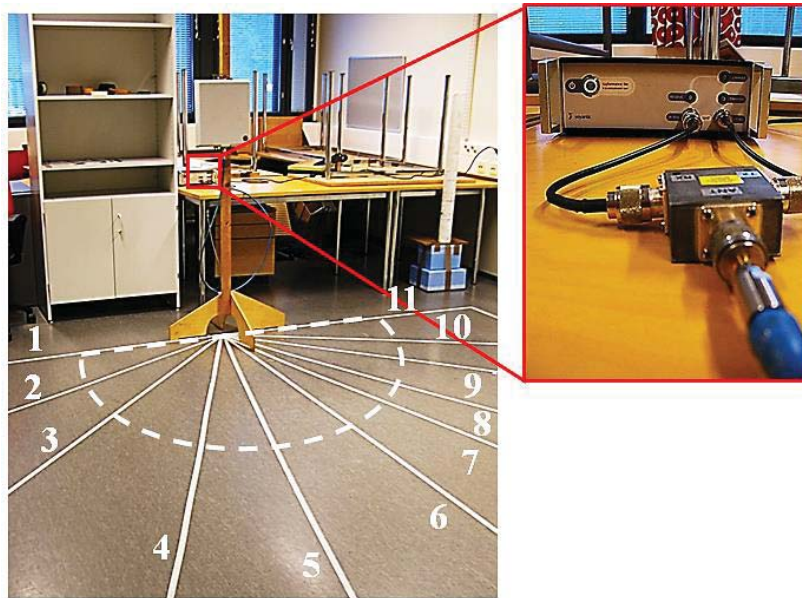


Figure 30. Electro-textile patch tag on-body RSS measurement set-up showing the 11 measurement lines.

The electro-textile patch tags were attached to the shirt similarly as in Fig. 29. The on-body RSS measurements were conducted along the 11 measurement lines. The received backscattered power from the on-body tags was recorded at 30-cm intervals from the reader antenna. For each measurement point, the main beam of the tag antenna was directed towards the reader antenna. All measurements were repeated 5 times. The recorded data was analyzed for different opening angles. Opening angle 1 includes the data from the measurement lines 5–7, angle 2 includes the data from the measurement lines 4–8, angle 3 includes the data from the measurement lines 3–9, angle 4 includes the data from the measurement lines 2–10, and angle 5 includes the data from the measurement lines 1–11. Opening angle 5 includes hence recorded RSS from all measurement points. Figure 31 plots the results for opening angels 1 and 5.

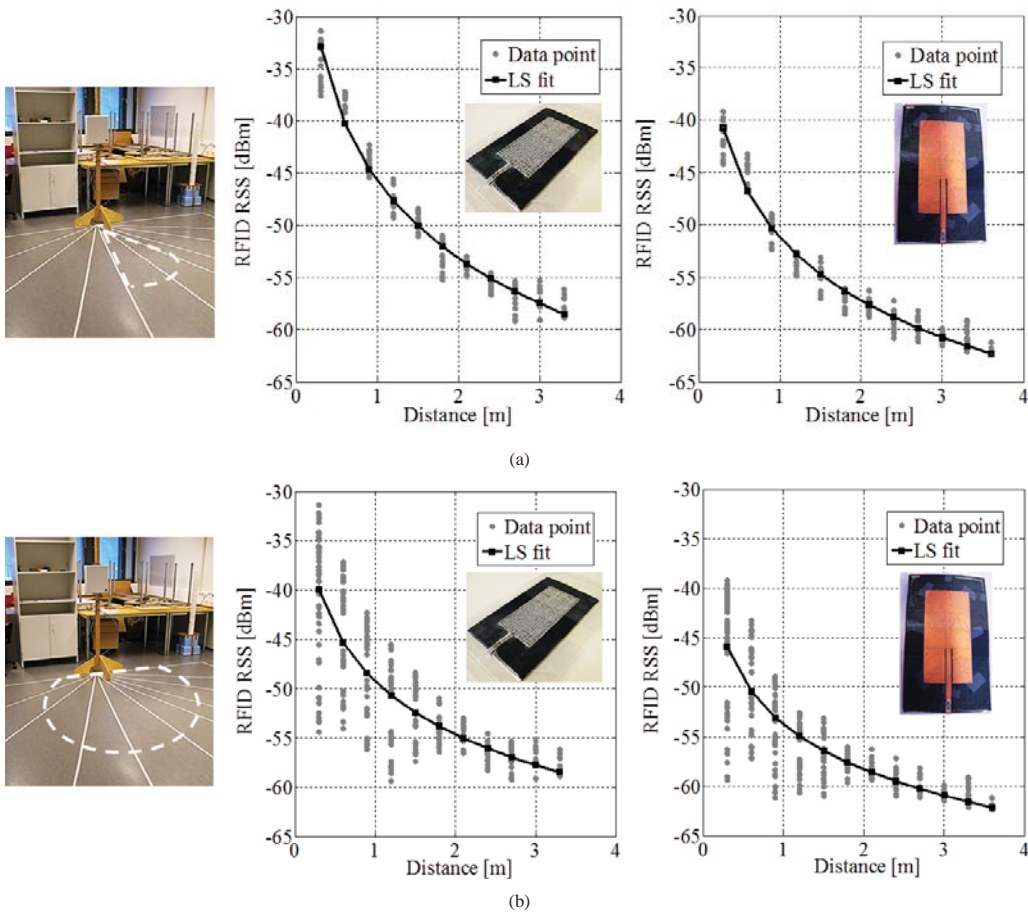


Figure 31. Backscattered power (RFID RSS) as a function of reader antenna to tag on-body distance  $d$  within opening angle (a) 1 and (b) 5. Least Square (LS) fit is applied to the measured data points.

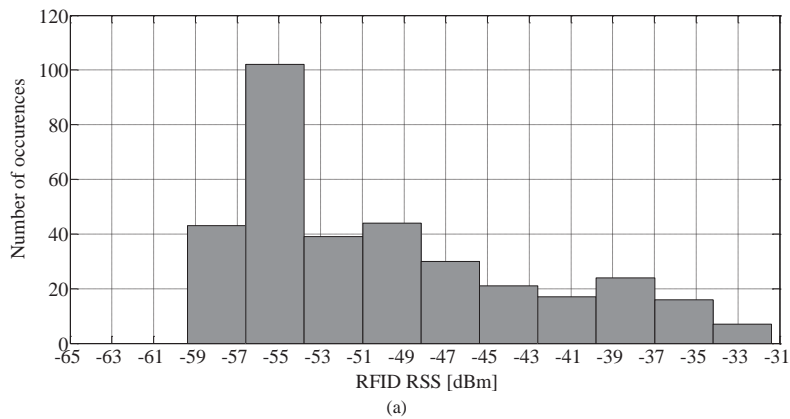
As expected, the recorded RSS from the passive RFID tags is low. Nevertheless, the robust tag antenna platform tolerance enables measurable RSS for distances  $d$  exceeding 3 meters. For opening angle 1, the on-body tag was maintained within the main beam of the reader antenna and the measurements were easily repeated. This resulted in a relative stable RSS for a given distance. When the opening angle was increased, measured RSS data from the measurement points located at wide angles caused variations in the recorded RSS for a given distance  $d$ . For these measurement points, the on-body tag was forced outside the main beam of the reader antenna and consequently, the RSS was degraded. Hence, recorded RSS for large distances  $d$  are mainly attained from measurement points located at small opening angles. The average standard deviation between the estimated (LS fit) RSS and the measured RSS data represents a metric for the backscattered RFID signal dynamics. Table 6 summarizes the average standard deviations for the opening angles 1–5.

Table 6. Opening angle average standard deviation; RFID RSS dynamics.

Opening angle	Embroidered patch tag [dB]	Copper fabric patch tag [dB]
1	1.55	1.29
2	1.62	1.35
3	2.62	2.02
4	3.70	2.87
5	4.28	3.35

The electro-textile patch tags perform similarly. The RFID RSS is very stable for small opening angles. For maximum opening angle, the signal dynamics is approximated 4 dB. Average standard deviations of 5–10 dB for similar indoor measurements with WLAN were reported in [93]. In terms of signal stability, the RFID RSS provides a competitive alternative to WLAN based localization. From Fig. 31 it is observed that the RFID RSS is saturated with increased distance  $d$ . However, within the defined observation area, the signal is not fully saturated. It is also observed that the copper fabric tag poses lower estimated RSS values compared to the embroidered tag, which is not in accordance with Fig. 29. However, when taking into account the measurement uncertainties and signal dynamics, it may be concluded that a higher read range in polarization-matched configuration does not guarantee higher RSS values.

The distribution of successfully recorded RFID RSS (Fig. 32) was used to conclude about the overall RFID signal quality within opening angle 5. Also here, it is observed that when the distance  $d$  is increased and the recorded RSS become low, a saturation (increased number of occurrences) in the recorded RSS is encountered.



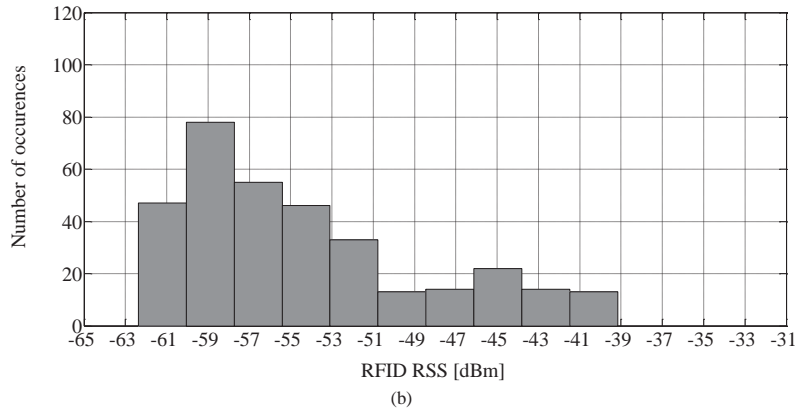


Figure 32. Distribution successfully recorded RFID RSS for opening angle 5 for the (a) embroidered and (b) copper fabric patch tags.

In summary, based on the RFID signal dynamics and quality analyses, the passive UHF RFID electro-textile patch tags have an enormous potential to provide a low-cost and low-complexity solution for indoor localization of people. The RSS-based RFID localization dynamics is dependent on the opening angle between the reader antenna and the body-worn antenna, and on the distance between the antennas. However, the results suggest that with an optimized RFID infrastructure that covers every point with minimal opening angle, a stable RFID signal is achievable. Such an infrastructure may be established by using several reader antennas deployed in the room and/ or by wearing multiple electro-textile antennas. The presented results help to understand the indoor wireless measurement channel behavior, which is required in order to understand the RFID signal propagation effects.

## 5 CONCLUSIONS

In the future, the human will be part of an intelligent infrastructure in which networked sensing and computing devices embed themselves into everyday objects in a transparent and an unobtrusive manner. The intelligent objects sense, interpret, and act on their environment, intercommunicate and change information with each other and with people. Ultimately, this seamless integration of computational intelligence into the world will recede into the background of our daily life. This is an essential consequence of the most profound technologies. Among the various technologies that potentially converge to this scenario, passive UHF RFID is one of the most promising candidates thanks to the energy autonomy of low-power battery-free tags. The technology is capable of offering long range identification and tracking of tagged entities and further, its low-cost enables widespread distribution and compatibility with disposal applications. Although the RFID technology has gained a foothold in the supply chain, ticketing, and asset tracking markets, it currently weaves itself into everyday life in the form of seamlessly integrated wearable tags with the goal of extracting information about human vital signs for the advancement of proactive healthcare management. Indeed, wearable passive UHF RFID holds the huge potential to bring the vision of pervasive wearable intelligence closer to reality.

Although wearable passive UHF RFID provides lightweight and transparent sensing resources that are easily integrated or shaped with clothing, its public acceptance still awaits. Two of the technology major challenges are the lack of powerful wearable tag antenna design parameters and optimization methodologies for the implementation of efficient and sophisticated RFID systems in close vicinity of the high-permittivity and dissipative human body. These challenges stem partly from the wearable tag antenna materials, electro-textile, that do not allow for traditional characterization and design methodologies due to their complex properties. In addition, the RF community lacks engineering tools that permit the fast and practical initiation of the design of optimized wearable tags near the human body. The research work presented in this thesis was conducted to specifically meet these demands.

In this thesis, it was shown that a highly practical statistical catalog of human body models can be generated time efficiently for the initiation of wearable UHF RFID tag designs by combining wireless measurement techniques with modern computational electromagnetics. The developed modeling technique for the human body is the single solution available today eliminating the need of a database of measured electrical parameters from tissue samples by exploiting the knowledge about measured on-body response from a reference tag of known characteristics in real scenario. The application of the modeling methodology for various body locations proved that such human body models are able to provide sufficient levels of accuracy in many wearable tag applications. A future catalog covering all possible body locations will enable a powerful RF tool for antenna designers to develop novel and sophisticated wearable antenna solutions for the promotion of intelligent wearable systems.

Next, the systematic and extensive analysis of various electro-textile patch antenna components confirmed the hypothesis that all electro-textiles applied as UHF antenna conductor exhibit dissipative dielectric characteristics. Consequently, from electro-textile antenna modeling point of view, a complex sheet impedance must be introduced to properly account for the electromagnetic effects related to the wearable antenna materials. For conductors the sheet impedance is purely real. For all embroidered electro-textiles, the sheet impedance is complex. It was evidenced that the sheet reactance accounts for the contributed tag antenna input inductance from the electro-textile. Since the power is limited in passive UHF RFID systems,



a common prime goal in tag design is to achieve proper tag antenna input impedance for the efficient power transfer at the tag antenna–IC interface at desired frequencies. For antennas with ground plane structures, robust platform tolerance is typically also demanded for higher directivities and hence, potentially longer operation ranges. These can be achieved by careful tag antenna design, use of well-characterized antenna materials, and exploiting proper optimization techniques. In this research work, an optimization methodology for the conductive thread distribution in embroidered antennas was for the first time proposed. It was proved that optimizing the thread distribution according to the simulated surface current density in a corresponding copper reference antenna, the electro-textile sheet impedance was minimized. Consequently, the embroidered antenna read range was maximized and the tag antenna impedance detuning was minimized. In addition, extremely robust antenna platform tolerance was achieved. Electro-textiles hold the enormous promise to provide flexible and light-weight wearable antennas that can be integrated with clothing already at the production lines, removing the need of separate antenna attachments. Particularly, the conductive sewing thread has the potential to become a natural raw material in the textile industry, enabling antennas that are seamlessly and unobtrusively integrated with clothing. These are important factors for the promotion of the technology industrial and public acceptance.

Finally, using the proposed optimization methodology, a flexible and fully embroidered wearable UHF RFID patch tag was designed and fabricated. The tag posed extremely low back lobe level, which provided excellent platform tolerance against the high-dielectric and dissipative human body. Furthermore, the tag achieved almost 4-meter read range in close vicinity of the human body, which sets a benchmark for future designs. This research work pointed out that in a dense infrastructure of reader antennas, the embroidered patch tag is capable of providing backscattered signals with small signal dynamics. In future, this capability could be utilized in RFID-inspired portable localization systems, in which the passive wearable tags enable the low-power and low-cost indoor localization of people in hospitals, schools, and other supervised premises.

As a final remark, this research work has, by the innovative use of material, novel analysis tools combined with computational electromagnetics, and by the development of powerful optimization methodologies, covered the entire design and fabrication procedure of the realization of advanced and novel wearable tag antennas, optimized to achieve excellent RF performance in close vicinity of the human body. The research work outcome form an important contribution to the state of the art and bring the vision of pervasive wearable intelligence closer to our reality.

## REFERENCES

*Author's publications supporting the thesis research work*

- [i] K. Koski, E. Koski, T. Björninen, A. A. Babar, L. Ukkonen, L. Sydänheimo, Y. Rahmat-Samii, "Practical read range evaluation of wearable embroidered UHF RFID tags," in *Proc. IEEE AP-S Int. Symp.*, 2 p., 2012.
- [ii] E. Moradi, K. Koski, L. Ukkonen, Y. Rahmat-Samii, T. Björninen, L. Sydänheimo, "Embroidered RFID tags in body-centric communication," *invited paper in Proc. IEEE iWAT*, pp. 362–365, 2013.
- [iii] K. Koski, E. Moradi, T. Björninen, L. Ukkonen, Y. Rahmat-Samii, "Truly wearable RFID tags for wireless body-centric identification and sensing systems," *invited paper in USNC-URSI National Radio Science Meeting*, 1 p., 2013.
- [iv] K. Koski, E. Moradi, T. Björninen, L. Sydänheimo, Y. Rahmat-Samii, L. Ukkonen, "On-body antennas: towards wearable intelligence," *invited paper in Proc. 31st URSI GASS*, 1 p., 2014.
- [v] K. Koski, E. Moradi, A. Vena, T. Björninen, L. Sydänheimo, L. Ukkonen, Y. Rahmat-Samii, "Characterization of electro-textiles using wireless reflectometry for optimization of wearable UHF RFID tags," *invited paper in Proc. PIERS*, pp. 1188–1192, 2013.
- [vi] T. Björninen, E. Moradi, K. Koski, L. Sydänheimo, L. Ukkonen, R. Muller, P. Ledochowitsch, J. M. Rabaey, Y. Rahmat-Samii, "Wearable and implantable antennas for wireless body-centric sensing systems," *invited paper in Proc. 8th BODYNETS*, 1 p., 2013.
- [vii] E. Moradi, K. Koski, T. Björninen, R. Muller, P. Ledochowitsch, L. Sydänheimo, E. Alon, M. M. Maharbiz, J. M. Rabaey, L. Ukkonen, Y. Rahmat-Samii, "Advances in implantable and wearable antennas for wireless brain-machine interface systems," *invited paper in USNC-URSI National Radio Science Meeting*, 1 p., 2014.
- [viii] S. Amendola, E. Moradi, K. Koski, T. Björninen, L. Sydänheimo, L. Ukkonen, J. M. Rabaey, Y. Rahmat-Samii, "Design and optimization of mm-size implantable and wearable on-body antennas for biomedical systems," *invited paper in Proc. 8th EUCAP*, 5 p., 2014.
- [ix] K. Koski, E. Moradi, T. Björninen, L. Sydänheimo, L. Ukkonen, Y. Rahmat-Samii, "Durability of embroidered antennas in wireless body-centric healthcare applications," *invited paper in Proc. 7th EUCAP*, pp. 565–569, 2013.
- [x] E. Koski, K. Koski, T. Björninen, A. A. Babar, L. Sydänheimo, L. Ukkonen, Y. Rahmat-Samii, "Fabrication of embroidered UHF RFID tags," in *Proc. IEEE AP-S Int. Symp.*, 2 p., 2012.

*References for theoretical background*

- [1] S. Mann, "Wearable computing: toward humanistic intelligence," *IEEE Intelligent Systems*, vol. 16, no. 3, pp. 10–15, 2001.
- [2] E. Welbourne, L. Battle, G. Cole, K. Gould, K. Rector, S. Raymer, M. Balazinska, G. Borriello, "Building the Internet of things using RFID: the RFID ecosystem experience," *IEEE Internet Computing*, vol. 13, no 3, pp. 48–55, 2009.
- [3] G. Kortuem, F. Kawsar, D. Fitton, V. Sundramoorthi, "Smart objects as building blocks for the Internet of things," *IEEE Internet Computing*, vol. 14, no. 1, pp. 44–51, 2010.
- [4] G. Acampora, D. J. Cook, P. Rashidi, A. V. Vasilakos, "A survey on ambient intelligence in healthcare," *Proc. IEEE*, vol. 101, no. 12, pp. 2470–2494, 2013.
- [5] D. Zhang, Z. Wang, B. Guo, Z. Yu, "Social and community intelligence: technologies and trends," *IEEE Software*, vol. 29, no. 4, pp. 88–92, 2012.
- [6] M. Weiser, "The computer for the 21st century," *Scientific American*, vol. 265, no. 3, pp. 66–75, 1991.
- [7] P. S. Hall, Y. Hao, *Antennas and Propagation for Body-Centric Wireless Communications*, 2nd ed., Norwood, MA: Artech House inc., 2012.
- [8] S. Movassaghi, M. Abolhasan, J. Lipman, D. Smith, A. Jamalipour, "Wireless body area networks: a survey," *IEEE Commun. Surveys Tuts.*, vol. PP, no. 99, pp. 1–29, 2014.
- [9] L. Zhang, Z. Wang, J. L. Volakis, "Textile antennas and sensors for body-worn applications," *IEEE Antennas Wireless Propag. Lett.*, vol. 11, pp. 1690–1693, 2012.
- [10] P. Bonato, "Wearable sensors and systems," *IEEE Eng. Med. Biol. Mag.*, vol. 29, no. 3, pp 25–36, 2010.
- [11] B.-R. Chen, S. Patel, T. Buckley, R. Rednic, D. J. McClure, L. Shih, D. Tarsy, M. Welsh, P. Bonato, "A web-based system for home monitoring of patients with Parkinson's disease using wearable sensors," *IEEE Trans. Biomed. Eng.*, vol. 58, no. 3, pp. 831–836, 2011.
- [12] X.-F. Teng, Y.-T. Zhang, C. C. Y. Poon, P. Bonato, "Wearable medical systems for p-health," *IEEE Rev. Biomed. Eng.*, vol. 1, pp. 62–74, 2008.
- [13] V. Stanford, "Pervasive computing goes the last hundred feet with RFID systems," *IEEE Pervasive Comput.*, vol. 2, no. 2, pp. 9–14, 2003.
- [14] M. Buettner, R. Prasad, M. Philipose, D. Wetherall, "Recognizing daily activities with RFID-based sensors," in *Proc. 11th UbiComp*, pp. 51–60, 2009.
- [15] M. Philipose, K. Fishkin, M. Perkowitz, D. Patterson, D. Fox, H. Kautz, D. Hahnel, "Inferring activities from interactions with objects," *IEEE Perv. Comput.*, vol. 3, no. 4, pp. 50–57, 2004.
- [16] F. Siegemund, C. Florkemeier, "Interaction in pervasive computing settings using bluetooth-enabled active tags and passive RFID technology together with mobile phones," in *Proc. 1st IEEE PerCom*, pp. 378–387, 2003.

- [17] S. Amendola, R. Lodato, S. Manzari, C. Occhiuzzi, G. Marrocco, "RFID technology for IoT-based personal healthcare in smart spaces," *IEEE Internet Things J.*, vol. PP., no. 99, 2014.
- [18] G. Roussos, V. Kostakos, "RFID in pervasive computing: state-of-the-art and outlook," *Pervasive and Mobile Computing*, vol. 5, no. 1, pp. 110–131, 2009.
- [19] H. Stockman, "Communication by means of reflected power," *Proc. IRE*, vol. 36, no. 10, pp. 1196–1204, 1948.
- [20] A. Vaz, A. Ubarretxena, I. Zalbide, D. Pardo, H. Solar, A. Gracia-Alonso, R. Berenguer, "Full passive UHF tag with temperature sensor suitable for human body temperature monitoring," *IEEE Trans. Circuits Syst. II, Exp. Briefs*, vol. 57, no. 2, pp. 95–99, 2010.
- [21] S. Manzari, A. Catini, C. Di Natale, G. Marrocco, "Ambient sensing by chemical-loaded UHF-RFIDs," in *Proc. 7th EUCAP*, pp. 1718–1720, 2013.
- [22] R. L. Shinmoto Torres, D. C. Damith, Q. Shi, A. P. Sample, "Sensor enabled wearable RFID technology for mitigating the risk of falls near beds," in *Proc. 7th IEEE RFID*, pp. 191–198, 2013.
- [23] D. Dobkin, *The RF in RFID: Passive UHF RFID in Practice*, Burlington, MA: Elsevier Inc., 2008.
- [24] F. Finkenzeller, *RFID Handbook: Fundamentals and Applications in Contactless Smart Cards and Identification*, 2nd ed., West Sussex: John Wiley & Sons Ltd., 2003.
- [25] International Organization for Standardization, ISO/IEC 18000-6, 2013: <http://www.iso.org/>.
- [26] EPCglobal Standards, 2013: <http://www.gs1.org/gsm/kc/epcglobal>.
- [27] NXP Semiconductors, UCODE G2iL series transponder ICs, 2014: <http://www.nxp.com/>.
- [28] Y. Yao, J. Wu, Y. Shi, F. F. Dai, "A fully integrated 900-MHz passive RFID transponder front end with novel zero-threshold RF–DC rectifier," *IEEE Trans. Ind. Electron.*, vol. 56, no. 7, pp. 2317–2325, 2009.
- [29] N. C. Wu, M. A. Nystrom, T. R. Lin, H. C. Yu, "Challenges to global RFID adoption," *Technovation*, vol. 26, no. 12, pp. 1317–1323, 2006.
- [30] S. L. Garfinkel, A. Juels, R. Pappu, "RFID privacy: an overview of problems and proposed solutions," *IEEE Security Privacy*, vol. 3, no. 3, pp. 34–43, 2005.
- [31] W. L. Stutzman, G. A. Thiele, *Antenna Theory and Design*, 2nd ed., Hoboken, NJ: John Wiley & Sons Inc., 1998.
- [32] J. L. Volakis, C.–C. Chen, K. Fujimoto, *Small Antennas: Miniaturization Techniques & Applications*, United States of America: McGraw-Hill Companies, 2010.
- [33] V. Lakafosis, A. Rida, R. Vyas, L. Yang, S. Nikolaou, M. M. Tentzeris, "Progress towards the first wireless sensor networks consisting of inkjet-printed, paper-based RFID-enabled sensor tags," *Proc. IEEE*, vol. 98, no. 9, pp. 1601–1609, 2010.
- [34] S. Manzari, C. Occhiuzzi, G. Marrocco, "Feasibility of body-centric systems using passive textile RFID tags," *IEEE Antennas Propag. Mag.*, vol. 54, no. 4, pp. 49–62, 2012.
- [35] T. Kellomäki, T. Björninen, L. Ukkonen, L. Sydänheimo, "Shirt collar tag for wearable UHF RFID systems," in *Proc. 4th EUCAP*, pp. 1–5, 2010.

- [36] C. A. Balanis, *Antenna Theory: Analysis and Design*, 3rd ed., Hoboken, NJ: John Wiley & Sons Inc., 2005.
- [37] P. Raunonen, L. Sydänheimo, L. Ukkonen, M. Keskilampi, M. Kivikoski, "Folded dipole antenna near metal plate," in *Proc. IEEE AP-S Int. Symp.*, vol. 1, pp. 848–851, 2003.
- [38] K. Koski, E. Koski, J. Virtanen, T. Björninen, L. Sydänheimo, L. Ukkonen, A. Z. Elsherbeni, Inkjet-printed passive UHF RFID tags: review and performance evaluation, *Int. J. Adv. Manuf. Technol.*, vol. 62, no. 1, pp. 167–182, 2012.
- [39] P. R. Foster, R. A. Burberry, "Antenna problems in RFID systems," *IEE Colloquium on RFID Technology*, pp. 3/1–3/5, 1999.
- [40] Y. C. Or, K. W. Leung, R. Mittra, K. V. S. Rao, "Analysis on the platform-tolerant radio-frequency identification tag antenna," *IET Microw. Antennas Propag.*, vol. 3, no. 4, pp. 601–606, 2009.
- [41] M. Hirvonen, P. Pursula, K. Jaakkola, K. Laukkanen, "Planar inverted-F antenna for radio frequency identification," *Electronic Letters*, vol. 40, no. 14, pp. 848–850, 2004.
- [42] M. Hirvonen, K. Jaakkola, P. Pursula, J. Säily, "Dual-band platform tolerant antennas for radio-frequency identification," *IEEE Trans. Antennas Propag.*, vol. 54, no. 9, pp. 2632–2637, 2006.
- [43] G. Kumar, K. P. Ray, *Broadband Microstrip Antennas*, Norwood, MA: Artech House, Inc., 2003.
- [44] T. V. Koskinen, H. Rajagopalan, Y. Rahmat-Samii, "A thin multi-slotted dual patch UHF-band metal-mountable RFID tag antenna," *Microw. Optical Tech. Lett.*, vol. 53, no. 1, 2011.
- [45] K. Kurokawa, "Power waves and the scattering matrix," *IEEE Trans. Microw. Theory Techn.*, vol. 13, no. 2, pp. 194–202, 1965.
- [46] T. Björninen, L. Sydänheimo, L. Ukkonen, "Development and validation of an equivalent circuit model for UHF RFIC IC based on wireless tag measurements," in *Proc. AMTA Symp.*, 6 p., 2012.
- [47] P. V. Nikitin, K. V. S. Rao, R. Martinez, S. F. Lam, "Sensitivity and impedance measurements of UHF RFID chips," *IEEE Trans. Microw. Theory Techn.*, vol. 57, no. 5, pp. 1297–1302, 2009.
- [48] G. Marrocco, "The art of UHF RFID antenna design: impedance-matching and size-reduction techniques," *IEEE Antennas Propag. Mag.*, vol. 50, no. 1, pp. 66–79, 2008.
- [49] J. Dacuna, R. Pous, "Low-profile patch antenna for RF identification applications," *IEEE Trans. Microw. Theory Techn.*, vol. 57, no. 5, pp. 1406–1410, 2009.
- [50] T. Björninen, K. Espejo Delzo, L. Ukkonen, A. Z. Elsherbeni, L. Sydänheimo, "Long range metal mountable tag antenna for passive UHF RFID systems," in *Proc. IEEE RFID-TA Int. Conf.*, pp. 194–198, 2011.
- [51] E. F. Knott, J. F. Shaeffer, M. T. Tuley, "Radar Cross Section, 2nd ed., Raleigh, NC: SciTech Publishing, Inc., 2004.
- [52] P. V. Nikitin, K. V. S. Rao, "Antennas and propagation in UHF RFID systems," in *Proc. IEEE RFID Int. Conf.*, pp. 277–288, 2008.
- [53] P. Pursula, M. Hirvonen, K. Jaakkola, T. Varpula, "Antenna effective aperture measurements with backscattering modulation," *IEEE Trans. Antennas Propag.*, vol. 55, no. 10, pp. 2836–2843, 2007.

- [54] P. V. Nikitin, K. V. S. Rao, "Theory and measurement of backscattering from RFID tags," *IEEE Antennas Propag. Mag.*, vol. 48, no. 6, pp. 212–218, 2006.
- [55] P. Pursula, D. Sandström, K. Jaakkola, "Backscattering-based measurement of reactive antenna input impedance," *IEEE Trans. Antennas Propag.*, vol. 56, no. 2, pp. 469–474, 2008.
- [56] C. Icheln, J. Krogerus, P. Vainikainen, "Use of balun chokes in small-antenna radiation measurements," *IEEE Trans. Instrum. Meas.*, vol. 53, no. 2, pp. 498–506, 2004.
- [57] E. Koski, T. Björninen, L. Ukkonen, L. Sydänheimo, "Radiation efficiency measurement method for passive UHF RFID dipole tag antennas," *IEEE Trans. Antennas Propag.*, vol. 61, no. 8, pp. 4026–4035, 2013.
- [58] G. Marrocco, E. D. Giampaolo, R. Aliberti, "Estimation of UHF RFID reading regions in real environments," *IEEE Antennas Propag. Mag.*, vol. 51, no. 6, pp. 44–57, 2009.
- [59] Voyantic, Ltd., Tagformance, 2014: <http://www.voyantic.com/>.
- [60] L. Ukkonen, L. Sydänheimo, M. Kivikoski, "Effects of metallic plate size on the performance of microstrip patch-type tag antennas for passive RFID," *IEEE Antennas Wireless Propag. Lett.*, vol. 4, pp. 410–413, 2005.
- [61] K. R. Carver, J. W. Mink, "Microstrip antenna technology," *IEEE Trans. Antennas Propag.*, vol. AP-29, no. 1, pp. 2–24, 1981.
- [62] D. M. Pozar, "Microstrip antennas," *Proc. IEEE*, vol. 80, no. 1, pp. 79–91, 1992.
- [63] ANSYS Simulation Software, HFSS, 2014: <http://www.ansys.com/>.
- [64] A. A. Babar, T. Björninen, V. A. Bhagavati, L. Sydänheimo, P. Kallio, L. Ukkonen, "Small and flexible metal mountable passive UHF RFID tag on high-dielectric polymer-ceramic composite substrate," *IEEE Antennas Wireless Propag. Lett.*, vol. 11, pp. 1319–1322, 2012.
- [65] H. Rajagopalan, Y. Rahmat-Samii, "Conformal RFID antenna design suitable for human monitoring and metallic platforms," in *Proc. 4th EUCAP*, pp. 1–5, 2010.
- [66] T. Kellomäki, J. Heikkinen, M. Kivikoski, "One-layer GPS antennas perform well near a human body," in *Proc. 2nd EUCAP*, pp. 1–6, 2007.
- [67] S. Manzari, C. Occhiuzzi, G. Marrocco, "Reading range of wearable textile RFID tags in real configurations," in *Proc. 5th EUCAP*, pp. 433–436, 2011.
- [68] I. Locher, M. Klemm, T. Kirstein, G. Tröster, "Design and characterization of purely textile patch antenna," *IEEE Trans. Advanced Packag.*, vol. 29, no. 4, pp. 777–788, 2006.
- [69] S. Zhu, R. Langley, "Dual-band wearable textile antenna on an EBG substrate," *IEEE Trans. Antennas Propag.*, vol. 57, no. 4, pp. 926–935, 2009.
- [70] J. Lilja, P. Salonen, T. Kaija, P. Maagt, "Design and manufacturing of robust textile antennas for harsh environments," *IEEE Trans. Antennas Propag.*, vol. 60, no. 9, pp. 4130–4140, 2012.
- [71] G. Marrocco, "RFID for the remote monitoring of human subjects," *IEEE Trans. Antennas Propag.*, vol. 55, no. 6, pp. 1862–1870, 2007.

- [72] M. A. Ziai, J. C. Batchelor, "Temporary on-skin passive UHF RFID transfer tag," *IEEE Trans. Antennas Propag.*, vol. 59, no. 10, pp. 3565–3571, 2011.
- [73] IFAC-CNR, Dielectric Properties of Body Tissues, 2012: <http://niremf.ifac.cnr.it/tissprop/htmlclie/htmlclie.htm>.
- [74] Peratech, QuantumTunnelling Composite, 2014: <http://www.peratech.com/>.
- [75] P. Stanley-Marbell, D. Marculescu, R. Marculescu, P. K. Khosla, "Modeling, analysis, and self-management of electronic textiles," *IEEE Trans. Comput.*, vol. 52, no. 8, pp. 996–1010, 2003.
- [76] Y. Ouyang, W. J. Chapell, "High frequency properties of electro-textiles for wearable antenna applications," *IEEE Trans. Antennas Propag.*, vol. 56, no. 2, pp. 381–389, 2008.
- [77] M. Polivka, M. Svanda, P. Hudec, "The optimization of the RFID system for the identification of sportsmen in mass races," in *Proc. EuMC*, pp. 732–735, 2007.
- [78] C. Hertleer, H. Rogier, L. Vallozzi, L. V. Langenhove, "A textile antenna for off-body communication integrated into protective clothing for firefighters," *IEEE Trans. Antennas Propag.*, vol. 57, no. 4, pp. 919–925, 2009.
- [79] Z. Wang, L. Zhang, Y. Bayram, and J. L. Volakis, "Embroidered conductive fibers on polymer composite for conformal antennas," *IEEE Trans. Antennas Propag.*, vol. 60, no. 9, pp. 4141–4147, 2012.
- [80] Shieldex, 110f34 dtex 2-ply HC, High Grade Multifilament Nylon Yarn, 2014: <http://statex.de/index.php/de/>.
- [81] E. Moradi, T. Björninen, L. Ukkonen, Y. Rahmat-Samii, "Effects of sewing pattern on the performance of embroidered dipole-type RFID tag antennas," *IEEE Antennas Wireless Propag. Lett.*, vol. 11, pp. 1482–1485, 2012.
- [82] S. Sankaralingam, B. Gupta, "Determination of dielectric constant of fabric materials and their use as substrates for design and development of antennas for wearable applications," *IEEE Trans. Instrum. Meas.*, vol. 59, no. 12, pp. 3122–3130, 2010.
- [83] LessEMF, EMF Shielding & Conductive Fabrics, 2014: <http://lessemf.com/>.
- [84] M. Toivonen, T. Björninen, L. Sydänheimo, L. Ukkonen, Y. Rahmat-Samii, "Impact of moisture and washing on the performance of embroidered UHF RFID tags," *IEEE Antennas Wireless Propag. Lett.*, vol. 12, pp. 1590–1593, 2013.
- [85] A. A. Babar, V. A. Bhagavati, L. Ukkonen, A. Z. Elsherbeni, P. Kallio, L. Sydänheimo, "Performance of high-permittivity ceramic-polymer composite as a substrate for UHF RFID tag antennas," *Int. Journ. Antennas Propag.*, vol. 2012, 8 p., 2012.
- [86] Wang, L. Zhang, J. L. Volakis, "Textile antennas for wearable radio frequency applications," *Textiles and Light Industrial Science and Technology*, vol. 2, no. 3, pp. 105–112, 2013.
- [87] S. Zhang, A. Chauraya, W. Whittow, R. Seager, T. Acti, T. Dias, Y. Vardaxoglou, "Embroidered wearable antennas using conductive threads with different stitch spacings," in *Proc. IEEE LAPC*, 4 p., 2012.

- [88] E. Moradi, T. Björninen, L. Ukkonen, Y. Rahmat-Samii, "Characterization of embroidered dipole-type RFID tag antennas," in *Proc. IEEE RFID-TA*, pp. 248–253, 2012.
- [89] Johannes Birkenstock GmbH, Wuppertal, Germany, 2013: [http://www.joh-birkenstock.de/index\\_en.html](http://www.joh-birkenstock.de/index_en.html).
- [90] D. Zhongliang, Y. Yanpei, Y. Xie, W. Neng, Y. Lei, "Situation and development tendency of indoor positioning," *China Commun.*, vol. 10, no. 3, pp. 42–55, 2013.
- [91] S. Shrestha, J. Talvitie, E. Lohan, "Deconvolution-based indoor localization with WLAN signals and unknown access point locations," in *Proc. ICL-GNSS*, pp. 1–6, 2013.
- [92] T. Sanpechuda, L. Kovavisaruch, "A review of RFID localization: applications and techniques," in *Proc. 5th ECTI-CON*, vol. 2, pp. 769–772, 2008.
- [93] E. S. Lohan, K. Koski, J. Talvitie, L. Ukkonen, "WLAN and RFID propagation channels for hybrid indoor positioning," in *Proc. ICL-GNSS*, 6 p., 2014.



Tampereen teknillinen yliopisto  
PL 527  
33101 Tampere

Tampere University of Technology  
P.O.B. 527  
FI-33101 Tampere, Finland

ISBN 978-952-15-3434-8  
ISSN 1459-2045